Peatland-VU-NUCOM (PVN 1.0): Using dynamic PFTs to model peatland vegetation, CH4 and CO2 emissions

Tanya J.R. Lippmann[1], Ype van der Velde[1], Monique M.P.D. Heijmans[2], Han Dolman[3,4], Dimmie M.D. Hendriks[5], and Ko van Huissteden[1,6]

[1]Vrije Universiteit, Amsterdam, the Netherlands
[2]Wageningen University and Research, Wageningen, the Netherlands
[3]Royal Netherlands Institute for Sea Research, Texel, the Netherlands
[4]Netherlands Earth System Science Center, Utrecht, the Netherlands
[5]Deltares Research Institute, Utrecht, the Netherlands
[6]VOF Kytalyk Carbon Cycle Research, Epse, the Netherlands

Correspondence: Tanya J.R. Lippmann (t.j.r.lippmann@vu.nl)

Abstract. Despite covering only 3% of the planet's land surface, peatlands store 30% of the planet's terrestrial carbon. The net greenhouse gas (GHG) emissions from peatlands depend on many factors but primarily soil temperature, vegetation composition, water level and drainage, and land management. However, many peatland models rely on water levels to estimate CH_4 exchange, neglecting to consider the role of CH_4 transported to the atmosphere by vegetation. To assess the impact of vegetation on the GHG fluxes of peatlands, we have developed a new model, Peatland-VU-NUCOM (PVN). The PVN model is a site-specific peatland CH_4 and CO_2 emissions model, able to reproduce vegetation dynamics. To represent dynamic vegetation, we have introduced plant functional types and competition, adapted from the NUCOM-BOG model, into the framework of the Peatland-VU model, a peatland GHG emissions model. The new PVN model includes plant competition, CH_4 diffusion, ebullition, root, shoot, litter, exudate production, below-ground decomposition, and above-ground moss development, under changing water levels and climatic conditions.

Here, we present the PVN model structure and explore the model's sensitivity to environmental input data and the introduction of the new vegetation-competition schemes. We evaluate the model against observed chamber data collected at two peatland sites in the Netherlands to show that the model is able to reproduce realistic plant biomass fractions, and daily CH_4 and CO_2 fluxes. We find that daily air temperature, water level, harvest frequency and height, and vegetation composition drive CH_4 and CO_2 emissions. We find that this process-based model is suitable to be used to simulate peatland vegetation dynamics, CH_4 and CO_2 emissions.

1 Introduction

Despite covering only 3% of the planet's land surface, peatlands store 30% (644 GtC) of the planet's terrestrial carbon (Yu et al., 2010). The present day global radiative effect of peatlands on the climate is estimated to be between -0.2 and -0.5 Wm^{-2} (i.e. a net cooling) (Frolking and Roulet, 2007), in comparison to a radiative forcing of +2.43 Wm^{-2} due to anthropogenic greenhouse gas (GHG) emissions since pre-industrial times (WGI, 2021). Future changes to the climate will impact the carbon

sequestration capacity of peatlands; however, the net effect of climate change on peatlands is not yet understood (Loisel et al., 2021). Research indicates that some peatlands will form a positive feedback (Dorrepaal et al., 2009); whist others will form a neutral (Saleska et al., 2002), or negative feedback to warming of the global climate system (Melillo et al., 2002; Lafleur et al., 2003) and the net effect of these complex responses is not yet known. The net warming effect of peatlands on the global climate system, and particularly the potential to both emit and drawdown CO_2 and CH_4, means that peatlands have a complex and multifaceted relationship with the global climate system.

The net GHG emissions from peatlands depends on many factors but primarily vegetation composition, land management, ground water level and drainage, and soil temperature (Dorrepaal et al., 2009; Tiemeyer et al., 2016). Rewetting drained peatlands is one strategy proposed to combat enhanced CO_2 emissions from peatlands but has been documented to both enhance and reduce GHG emissions (eg. Günther et al. (2020); Boonman et al. (2022)) with the majority of studies concluding that rewetting leads to enhanced CH_4 and net GHG emissions (Harpenslager et al., 2015; Knox et al., 2015). Field studies have shown that vegetation restoration in combination with rewetting may reduce GHG emissions (Graf and Rochefort, 2009; Mazzola et al., 2022). Vegetation impacts the net GHG emissions in peatlands by directly influencing the net primary production and organic matter available for decomposition and indirectly, by influencing the substrates available for microbial metabolisation in the soil column (Bansal et al., 2020; Bridgham et al., 2013).

While the effects of groundwater table on peatland GHG emissions are extensively described (Evans et al., 2021), the impacts of plant type and plant community composition on GHG emissions are less understood (Malmer et al., 2003). Changes in vegetation composition have been observed in long running water table manipulation experiments (Peltoniemi et al., 2009; Strack et al., 2006). Generally, sedges and mosses establish during wetter conditions and shrubs and trees develop during drier conditions, with enhanced *Sphagnum* growth out-competing shrubs during warming experiments (Dorrepaal et al., 2006). Below-ground, changes in vegetation have been accompanied by changes in bacterial and fungal biomass (Jaatinen et al., 2008), and methanogenic and methanotrophic community diversity (Yrjälä et al., 2011; Lippmann et al., 2021). Changes to CO_2 (NPP) have been observed following changes in plant community composition, further impacting root exudation (Ballantyne et al., 2014). Root exudates are a diverse group of organic compounds secreted by plant roots into the nearby soil. The composition and quality of root exudates varies between plant types, influencing microbial community composition and function, CO_2 (Crow and Wieder, 2005) and CH_4 fluxes (Schipper and Reddy, 1996). Plant growth, root exudation and decomposition of organic matter happen at rates that differ depending on plant type (Dorrepaal et al., 2007). *Sphagnum* is a primary contributor to the carbon sequestration in many peatlands and decomposes three times slower than most vascular plants (Graf and Rochefort, 2009). Spatial variation in the rate of vegetation growth and decomposition, particularly for bryophyte species, leads to the creation of microforms, such as hummocks, hollows and lawns which in turn impact the water level relative to the surface and spatially variable fluxes (Waddington and Roulet, 2000). Differences in vegetation composition within the same site and with the same water levels have been observed to lead to differences in CH_4 fluxes (Bubier, 2016; Jackowicz-Korczyński et al., 2010). To understand the role of vegetation emissions' feedbacks during peatland restoration efforts, vegetation must thus be treated as a dynamic interactive element of the peatland ecosystem.

Plants with common ecosystem functions or structures can be represented with common model algorithms or parameters in a vegetation model when grouped as Plant Functional Types (PFTs) (Wullschleger et al., 2014). Plant functional types have been found to explain uncertainties in GHG emissions from wetlands in response to warming in a meta-analysis of wetlands exposed to warming (Bao et al., 2023). Dynamic (rather than static) PFTs simulate the inter-seasonal growing and dying of plants, that over a number of years lead to vegetation succession, and are critical to reliably assess the impacts of climate and environmental change on peatland ecosystems (Box et al., 2019). Shifts in community composition lead to feedbacks between species and other environmental parameters such as soil moisture, bulk density, soil organic matter (SOM) content, gas conduit function, rate of growth, rate of decomposition, microbial mineralisation, and aerobic decomposition (De Boeck et al., 2011). Dynamic plant representation is critical to reliably simulate vegetation-environmental feedbacks in models (Toet et al., 2006) and therefore, the inclusion of dynamic vegetation classes is critical to reliably estimate C, CO_2 and CH_4 emissions from peatlands during periods of environmental change (Li et al., 2016; Laine et al., 2022).

Many peatland carbon cycle models have been developed over the preceding decades. The Wetland and Wetland CH_4 Inter-comparison of Models Project (WETCHIMP) evaluated the ability of a variety of models to simulate large-scale wetland characteristics and corresponding CH_4 emissions (Melton et al., 2013; Wania et al., 2013). Peatland modelling efforts have made significant advancements to simulate CH_4 fluxes by including CH_4-specific processes such as CH_4 plant transport and ebullition. However, many models rely on CO_2 fluxes or surface water levels as indicators of CH_4 exchange (Metzger et al., 2015), restricting their capacity to assess feedbacks between environmental change and the peatland CH_4 cycle. There exist two pre-existing models that simulate dynamic vegetation, CO_2, and CH_4 cycling in peatlands (i.e. PEATBOG (Wu et al., 2016) and LPJ-WHyMe (Wania et al., 2010)) thereby, limiting the ability of the modelling community to assess model mechanistic processes. The functionality and scope of current models that simulate peatlands and include either dynamic or static vegetation are compared in Table S1. The PEATBOG model simulates three PFTs, moss, shrubs, and graminoids at the Mer Bleue Bog site, and represents a comprehensive array of peatland processes, including the nitrogen cycle and dissolved gases (carbon, CO_2, and CH_4). LPJ-WHyMe, like its parent model, LPJ-WHy (Sitch et al., 2003; Gerten et al., 2004), includes permafrost and peatlands, two peatland-specific PFTs (flood tolerant C_3 graminoids and *Sphagnum* mosses), a new decomposition scheme when under inundation, and the addition of root exudates. LPJ-WHyMe particularly assesses the impacts of inundation on vegetation composition, net primary production, and the deceleration of decomposition under inundation.

To assess the impact of dynamic vegetation classes on subsequent GHG fluxes in peatlands we present a new model, Peatland-VU-NUCOM v1.0 (PVN). PVN incorporates features of NUCOM-BOG, a bog ecosystem model (Heijmans and Berendse, 2008), into the Peatland-VU model framework, a process-based peatland model (van Huissteden et al., 2006). The NUCOM-BOG model simulates vegetation competition, C, nutrient, and water cycling in undisturbed bog ecosystems under changing climates, using a soil profile divided by an acrotelm-catotelm boundary where plant growth and decomposition are partitioned between plant organs. The Peatland-VU model simulates the CH_4 and CO_2 cycle within a column of peat soil with varying water levels. The Peatland-VU model simulates CH_4 fluxes, gross primary productivity and CO_2 cycle whilst assuming a constant plant layer and does not include a nitrogen cycle. We have developed a model that, with the appropriate site input data, can be used to simulate peatland sites with a wide variety of vegetation types and vegetation management

practices. For this reason, there is no limit to the number of PFTs that can be included in a model simulation. The inclusion of dynamic vegetation classes into the PVN model provides a model that is capable of estimating the greenhouse gas balance in response to environmental changes (changes in temperature, radiation, precipitation/evapotranspiration or water levels) and also different management efforts (changes in harvest regime or vegetation restoration) for peatland sites. The incorporation of NUCOM-BOG features, a model simulating undisturbed systems, into PVN, a new model simulating disturbed and managed systems, requires that changing environmental conditions and changing management practices both lead to dynamic impacts on vegetation classes. Therefore, this model can serve wetland management by estimating changes in the greenhouse gas balance of peatland sites in response to management decisions, whilst considering effects of environmental change.

2 Materials and Methods

2.1 The PVN model

The new PVN model describes the vegetation, CH_4 and CO_2 dynamics of a column of an above- and below-ground peatland ecosystem (Fig. 1). Carbon dioxide and CH_4 emissions enter the atmosphere by ebullition, transport through plants, diffusion through the soil, and respiration. The above-ground carbon pools are above-ground living biomass, litter layer (non-moss PFTs only), shoots, and living moss depth (moss PFTs only). The below-ground carbon pools are peat, labile organic matter, microbial biomass, litter & dead roots, and root exudates (Table S2).

Plant Functional Types (PFT) are the key element of NUCOM that is added to the Peatland-VU framework to create the PVN model. Any number of PFTs can be included in a model simulation. PFT attributes (parameters) describe plant physiology and bioclimatic limits. Bioclimatic limits are used by the photosynthesis function (Sect. 2.1.1), and the potential growth function (Eq. 13). Each PFT is defined as being either a moss or vascular plant type which impacts the ability of plants to grow vertically or develop roots. Each PFT is prescribed as having either evergreen or deciduous phenology. For deciduous vegetation, leaf senescence increases when the daily temperature falls below the PFT's minimum tolerated temperature whereas, for evergreen vegetation, leaf senescence refers to the death of old leaves (Eq. 9). Maximum leaf coverage is maintained as long as daily water level and temperature are within the ideal range. The PFT parameters are defined in Table 1 and the references are listed in Table S3, respectively. In this section, the subscript, p, is used to show that the equation or variable is PFT specific, z to indicate that the equation or variable is soil layer specific, t to represent time, T represents temperature, and WL represents water level. The convention used in this manuscript is that a positive flux represents the movement of gas from the ecosystem to the atmosphere.

2.1.1 Primary production

C3 photosynthesis, leaf respiration (RT), and net primary production (NPP) are calculated using a modified version of the primary production scheme introduced into the Peatland-VU model by Mi et al. (2014), modified from the BIOME3 equilibrium biosphere model Haxeltine and Prentice (1996). The BIOME3 model is based on the premise that GPP and leaf respiration

Table 1. Name, units, description and values of PFT input parameters. Associated references are listed in Table S3. In the left column each PFT parameter is tied to its relevant model mechanism. Note that some PFT parameters are, at times, used by multiple model processes.

Corresponding model process	Parameter	Units	Description	Tall grass	Sedges	*Typha*	*Sphagnum*	Brown moss	Short grass
Above-ground biomass	BS	-	Fraction of above-ground biomass converted to litter	0.04	0.04	0.04	0.01	0.015	0.03
	KL	-	Fraction of biomass converted to litter during autumn, for deciduous plants	0.1	0.1	0.1	0.01	0.04	0.06
	CBiomassRatio	-	Carbon to biomass ratio	0.46	0.46	0.46	0.44	0.44	0.44
	RS	-	Fraction of growth that consists of shoots. Remainder is root growth	0.7	0.7	0.7	1.0	1.0	0.9
	MaxCanopyHeight	m	Maximum height	1.5813	2.5813	2.5813	0.1	0.2	0.4
Photosynthesis & respiration	$T_{MaxPhoto}$	°C	Maximum temperature for photosynthesis	38	40	35	30.0	30.0	30
	$T_{MinPhoto}$	°C	Minimum temperature for photosynthesis	-3	-1	-3	-1.0	0.5	-1
	T_{min}	°C	Minimum temperature for growth	7	2	2	-1.0	0.5	0.5
	T_{minopt}	°C	Lowest temperature for optimal growth	9	12	12	14.0	5.0	14
	T_{maxopt}	°C	Highest temperature for optimal growth	20	30	30	25.0	25.0	25
	T_{max}	°C	Maximum temperature for growth	45	45	45	38.0	38.0	38
	Rc	-	Leaf maintenance respiration coefficient	0.015	0.015	0.015	0.016	0.014	0.014
	Rr	-	Leaf respiration coefficient	0.015	0.015	0.015	0.016	0.014	0.014
	Gmax	$gCday^{-1}$	Maximum growth rate	0.07	0.07	0.07	0.045	0.05	0.05
LAI	SLA	$m^2\,g^{-1}$	Ratio of leaf area to dry leaf mass	0.012	0.012	0.012	0.02	0.02	0.02
	MinLAI	$m^2\,m^{-2}$	Minimum LAI	0.1	0.1	0.1	0.1	0.1	0.1
	MaxLAI	$m^2\,m^{-2}$	Maximum LAI	3	4	4	1.2	1.5	1.5
	LEC	-	Light extinction coefficient	0.5	0.46	0.5	0.95	0.95	0.95
CH_4 scheme	PlOx	-	Fraction of CH_4 consumed by rhizospheric oxidation	0.4	0.4	0.25	0.7	0.8	0.6
	vP	-	Vegetation type factor for gas transport through plants	5	6	10	2.0	2.0	2
Root processes	MRD	m	Maximum root depth	0.46	1	1	0.1	0.1	0.2
	RSX	day^{-1}	Proportion of root mass that dies during each time step	0.05	0.05	0.05	0.01	0.01	0.05
	REX	-	Fraction of below-ground production that consists of exudates	0.1	0.2	0.2	0.0	0.0	0.11
	KSP	-	Coefficient for stronger exudation in spring	0.2	0.4	0.4	0.0	0.0	0.1
Below-ground decomposition	LC	day^{-1}	Conversion factor of above-ground to below-ground litter. 0 °C, LC is set to 0.	0.005	0.001	0.001	0.01	0.005	0.003
	HU	-	Fraction of decomposed organic material transferred to resistant humus fraction	0.55	0.42	0.3	0.9	0.9	0.9
	MI	-	The amount of carbon from decomposed organic matter converted to microbial biomass	2.25	2.2	2.2	2.4	2.3	2.3
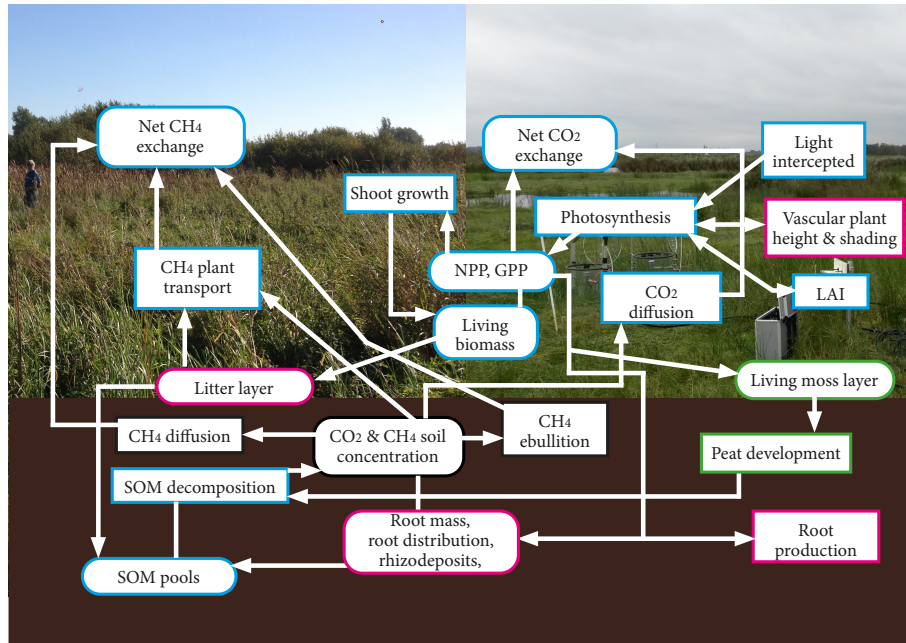
Figure 1. Schematic of the movement of carbon in the model. Processes are delineated with rectangles, whereas carbon pools are delineated with curved edges. The pink outline represents non-moss pools and processes, green outline represents pools and processes applicable only to moss PFTs and the blue outline refers to pools and processes that are applicable for all plant types. In the background of this figure, the Horstermeer site is shown on the left and the Ilperveld on the right.

Table 1. Continued.

Corresponding model process	Parameter	Units	Description	Tall grass	Sedges	*Typha*	*Sphagnum*	Brown moss	Short grass
Water level	WL_{min}	m	Minimum water level for growth	-1	-1	-1	-0.5	-0.35	-0.35
	WL_{minopt}	m	Lowest water level for optimal growth	-0.4	-0.3	-0.4	-0.2	-0.15	-0.15
	WL_{maxopt}	m	Highest water level for optimal growth	-0.2	-0.2	0	-0.05	-0.05	-0.05
	WL_{max}	m	Maximum water level for growth	0.0192	0.1	0.3	0.05	0.05	0.05

increase with the activity of (Rubisco) photosynthetic enzymes in leaf chloroplasts. Photosynthesis is calculated using stomatal conductance and Rubisco activity of leaves. The net CO_2 fluxes (NEE) for each PFT are the sum of gross primary production (GPP [kg C m^{-2} day^{-1}]), minus plant respiration, CO_2 produced by below-ground aerobic SOM decomposition, and CO_2 oxidised from CH_4 (Rox).

$$GPP_{t,p} = \frac{JE_{t,p} + JC_{t,p} - \sqrt{(JE_{t,p} + JC_{t,p})^2 - 4 \cdot JE_{t,p} \cdot JC_{t,p}}}{20 \cdot WSF_{t,p}} \tag{1}$$

where, JE [kg C m^{-2} day^{-1}] describes the relationship of photosynthesis to photosynthetically active radiation (PAR) and JC [kg C m^{-2} day^{-1}] describes the Rubisco limited rate of photosynthesis. JE and JC are defined by Eq. S2 and Eq. S10, respectively (Haxeltine and Prentice, 1996; Mi et al., 2014). Interactions among leaf area development, photosynthetic activity,

130 stomatal conductance, temperature and water availability have been widely recognised (Baldocchi and Harley, 1995; Koebsch et al., 2020). Water stress has a significant impact on plant photosynthetic capacity (Keenan et al., 2010). Studies such as Ostle et al. (2009); Puma et al. (2013) have considered these factors when simulating GPP by introducing water use efficiency terms. Model intercomparison efforts have found improved reproducibility of GPP estimates from models that account for the impacts of water stress on photosynthetic capacity (De La Motte et al., 2020; Churkina et al., 1999). GPP in the PVN model is modified

135 by both a water stress factor (WSF [-], Eq. S1) and a temperature stress factor (ϕ_T, Eq. S4, adapted from Mi et al. (2014)).

$$NPP_{t,p} = GPP_{t,p} - \int_{z}^{0} Rd_{t,p} dz - RT_{t,p} \qquad (2)$$

where, NPP represents the net primary productivity [kg C m^{-2} day^{-1}], RT [kg C m^{-2} day^{-1}] represents daily leaf respiration, and Rd [kg C m^{-3} day^{-1}] represents the root respiration (Eq. 16). Total daily root respiration is the sum of root growth which varies with depth and is dependent on the root distribution (17).

140 $$RT_{t,p} = Rr_p \cdot VM_{t,p} \qquad (3)$$

where, Rr [-] is the leaf respiration coefficient (Table 1), and VM [kg C m^{-2} day^{-1}] represents the maximum daily rate of net photosynthesis (Eq. S11, Haxeltine and Prentice (1996); Mi et al. (2014)). The CO_2 flux from each soil layer (B_{CO_2}) is calculated before integrating over all layers and summed with CO_2 produced by decomposed litter (LLd [kg C m^{-2} day^{-1}]), and NPP is subtracted.

145 $$NEE_{t,p} = \int_{z}^{0} B_{CO_2,t,p,z} dz + LLd_{t,p} - NPP_{t,p} \qquad (4)$$

where, NEE [kg C m^{-2} day^{-1}] is the Net Ecosystem Exchange, B_{CO_2} [kg C m^{-3} day^{-1}] is the CO_2 flux produced by below-ground SOM decomposition (Eq. 27).

2.1.2 Competition among PFTs

Biomass fraction (BF) is a representation of the ratio of PFT biomass to total biomass (Eq. 5). The sum of all PFTs is

150 constrained to a maximum BF of 1.0. All PFTs have a minimum BF of 0.1 and are able to further establish when the conditions

7

become favourable, as adapted from the NUCOM-BOG model (Heijmans and Berendse, 2008).

$$BF_{t,p} = \frac{CB_{t,p}}{\sum_{p=1}^{P}(CB_{t,p})} \tag{5}$$

where, CB [kg C m^{-2}] represents above-ground living biomass (Eq. 9). Each plant competes for light where taller PFTs have monopoly over shorter PFTs. Light that is not intercepted by the tallest PFT, becomes available to the next PFT, in descending

155 height order. Light which is not intercepted by the vascular PFTs ($_v$) is passed on and divided between moss PFTs ($_{mp}$), proportional to their BF. In this way, an increase of foliage of taller PFTs may reduce the growth rates of mosses due to shading by limiting light exposure. Each time step, vascular PFTs are ordered according to descending height so that the shading by taller PFTs impacts the amount of light available to shorter PFTs. The height of vascular PFTs is calculated using an allometric relationship (Eq. 6) adapted from Huang et al. (1992); Smith et al. (2001); Krinner et al. (2005) which relates vegetation

160 biomass to height. This relationship, initially intended to be used for trees, has since been used to calculate the heights of natural and agricultural grasses in a dynamic global vegetation model (Krinner et al., 2005). Biomass and stem density have been found to respectively explain 98% and 81% of the height variance in 65 plots of 29 different species (Gorham, 1979) because most plants are understood to be constrained by 'self-thinning' under crowding in natural stands, or by a trade-off between height and foliage growth, reflecting a trade-off between structural and functional physiological development.

165 $$H_{t,v} = k_2 \cdot \left(\frac{4 \cdot CB_{t,v}}{BD \cdot \pi \cdot k_2} \right)^{\frac{k_3}{2+k_3}} \tag{6}$$

where, H refers to plant height [m], BD represents biomass density [kg C m^{-3}], k_2 [m], and k_3 [-] are constants with values 40, and 0.85, taken from Smith et al. (2001). $FPAR$ [-] is the fraction of incoming PAR absorbed by vegetation (Eq. 7) and is dependent on LAI and the amount of shading by taller plants.

$$FPAR_{t,p} = 1 - e^{(-LEC_p \cdot LAI_{t,p})} \tag{7}$$

170 Where, LEC represents the Light Extinction Coefficient parameter [-]. LAI [m^2 m^{-2}] is calculated as a function of living biomass and the Specific Leaf Area (SLA [m^2 kg^{-1} C]).

$$LAI_{t,p} = \begin{cases} MinLAI_p, & \text{if } LAI_{t,p} < MinLAI_p \\ CB_{t,p} \cdot SLA_p, & \text{if } MinLAI_p \leq LAI_{t,p} \leq MaxLAI_p \\ MaxLAI_p, & \text{if } LAI_{t,p} > MaxLAI_p \end{cases} \tag{8}$$

where, CB [kg C m^{-2}] represents above-ground living biomass (Eq. 9), dependent on shoot growth and biomass senescence lost to the litter layer.

$$\frac{\delta}{\delta t} CB_{t,p} = SM_{t,p} - BS_{t,p} \cdot CB_{t,p} \tag{9}$$

where, SM represents shoot mass [kg C m^{-2} day^{-1}], calculated using Eq. 10, and $BS_{t,p}$ represents the fraction of above-ground biomass littered each day [day^{-1}]. Biomass senescence, BS_p [day^{-1}], is set to KL_p [day^{-1}] during Autumn, for deciduous plants.

$$SM_{t,p} = RS_p \cdot NPP_{t,p} \tag{10}$$

where, RS [-] represents the ratio of shoot to root growth (Table 1). The allocation of root and shoot growth is a fixed fraction of NPP so that the fraction of shoot and root growth sums to 1.0. Growth of moss PFTs (HG, Eq. 11) is represented in terms of fractional cover, rather than height. A moss PFT with more cover has access to more light and gains an advantage over other mosses. Moss PFTs develop at different rates due to differences in the range of temperatures, and water levels needed for growth. The depth (or thickness, [m]) of both individual moss PFTs (Eq. 11), and the total living moss layer (Eq. 12) are dependent on BF, potential growth, and dry bulk density (DBD, kg C m^{-3}). The thickness of the living moss layer is not yet used by the model. Future model versions will use the thickness of the moss layer to recalculate land surface height, impacting the water level relative to the surface and also soil properties (such as DBD, pH, OM content of top soil layer(s)).

$$HG_{t,mp} = \frac{PG_{t,mp} \cdot BF_{t,mp}}{DBD_{t,mp,z=1}} \tag{11}$$

where, $_{mp}$ represents moss PFTs only, PG represents potential growth (PG [-], Eq. 13). The moss thicknesses of individual moss PFTs are aggregated to calculate the total ecosystem moss depth (MHG [m]):

$$MHG = \frac{\sum_{mp=1}^{MP}(HG_{t,mp} \cdot BF_{t,mp})}{\sum_{mp=1}^{MP} BF_{t,mp}} \tag{12}$$

Potential growth (PG [-], Eq. 13) reflects the favourability of water levels or temperatures for PFT growth, calculated using the water growth, WG [-], and temperature growth, TG [-] functions, respectively. Potential growth, WG, and TG are adapted functions from Heijmans and Berendse (2008).

$$PG_{t,p} = FPAR_{t,p} \cdot Gmax_p \cdot TG_{t,p} \cdot WG_{t,p} \tag{13}$$

where, $Gmax$ is the maximum growth rate [kg C m^{-2} day^{-1}]. The WG and TG functions are congruent to each other, where unfavourable temperature or water levels reduce growth.

$$WG_{t,p} = \begin{cases} 0, & \text{if } WL_t < WL_{min,p} \\ \frac{WL_t - WL_{min,p}}{WL_{minopt,p} - WL_{min,p}}, & \text{if } WL_{min,p} \leq WL_t < WL_{minopt,p} \\ 1, & \text{if } WL_{minopt,p} \leq WL_t \leq WL_{maxopt,p} \\ \frac{WL_{max,p} - WL_t}{WL_{max,p} - WL_{maxopt,p}}, & \text{if } WL_{maxopt,p} < WL_t \leq WL_{max,p} \\ 0, & \text{if } WL_t > WL_{max,p} \end{cases} \tag{14}$$

where, WL refers to water level, min and max refer to the minimum and maximum water levels tolerated for growth, $minopt$ and $maxopt$ refer to minimum and maximum optimum water levels for growth, respectively.

$$TG_{t,p} = \begin{cases} 0, & \text{if } T_t < T_{min,p} \\ \frac{T_t - T_{min,p}}{T_{minopt,p} - T_{min,p}}, & \text{if } T_{min,p} \leq T_t < T_{minopt,p} \\ 1, & \text{if } T_{minopt,p} \leq T_t \leq T_{maxopt,p} \\ \frac{T_{max,p} - T_t}{T_{max,p} - T_{maxopt,p}}, & \text{if } T_t \leq T_{max,p} \\ 0, & \text{if } T_t > T_{max,p} \end{cases} \tag{15}$$

where, T refers to daily temperature, min and max refer to the minimum and maximum tolerated temperatures for growth, $minopt$ and $maxopt$ refer to minimum and maximum optimum temperatures for growth, respectively.

2.1.3 Below-ground production

The root distribution, and root mass of vascular PFTs are mapped to the layout of the model's soil horizon representation (depth, density, layer thickness). To account for differences in decomposition rates among roots, and exudates, each PFT has designated SOM pools, which are partitioned between the soil layers. Root distribution, and root mass decrease exponentially from the surface to the PFT maximum root depth (MRD in Table 1). In general, 30%, 50%, and 75% of roots are observed in the top 10 cm, 20 cm, and 40 cm, respectively (Jackson et al., 1996). Root exudation plays an important role in the rhizosphere by promoting methanogensis and soil carbon loss through CH_4 production. The production of new roots (Rd) is based on a PFT prescribed shoot to root growth ratio and NPP. Root exudates (RX, Eq. 19) are a fraction of calculated below-ground root production (Rd). Exudates develop at a prescribed rate per PFT, dependent on root and shoot growth. Photosynthesis rates are enhanced during spring and summer and are accompanied by the highest levels of root and soil respiration (Högberg et al., 2001). There is strong evidence to suggest that enhanced photosynthesis fuels exudate production, causing seasonal variation in exudation (Whipps, 1990; Saarnio et al., 2004). The root growth and die off functions are adapted from van Huissteden et al.

(2006).

$$Rd_{t,v,z} = (1 - RS_v) \cdot NPP_{t,v} \cdot f(z,p) \tag{16}$$

where, 1 - RS represents the fraction of growth that is root growth, $f(z,p)$ [m^{-1}] represents the exponential root distribution from the surface to maximum root depth (MRD in Table 1).

$$\int_{-MRD_p}^{0} f(z,p)dz = 1 \tag{17}$$

$$\frac{\delta}{\delta t} RM_{t,v,z} = Rd_{t,v,z} - RX_{t,v,z} - RDR_{t,v,z} \tag{18}$$

where, RM is the root mass [kg C m^{-3}]. RDR [kg C m^{-3} day^{-1}] represents the death of existing roots.

$$RX_{t,v,z} = Rd_{t,v,z} \cdot f(KSP_{v,DoY}) \cdot REX_{t,v} \tag{19}$$

where, DoY represents the day of the year, REX [-] represents the unitless root exudation factor, and $f(KSP)$ [-] is a function depending on PFT constant, KSP (Table 1), that can be used to determine stronger exudation occurs during spring.

$$RDR_{t,v,z} = RM_{t,v,z} \cdot RSX_v \tag{20}$$

where RSX represents the root senescence rate [day^{-1}].

2.1.4 Litter layer production and decomposition

Vegetation composition change directly impacts litter inputs, which alters the quality and quantity of fresh SOM contributions (Malmer et al., 2005). Senescence of the above-ground living biomass is added to the litter layer, for vascular PFTs (Eq. 21). Senescence of moss PFTs contributes directly to the below-ground SOM pools. Movement of surface litter to SOM pools, is an important component of peatlands (Davidson and Janssens, 2006). Carbon dioxide produced from the decomposition of the litter layer and the different SOM pools are summed with NEE (Eq. 4).

$$\frac{\delta}{\delta t} LL_{t,v} = LLp_{t,v} - LLl_{t,v} - LLd_{t,v} \tag{21}$$

11

where,

$$LLp_{t,v} = BS_v \cdot CB_{t,v} \tag{22}$$

$$LLl_{t,v} = \frac{T_t}{KT} \cdot LC_p \cdot LL_{t,v} \tag{23}$$

$$LLd_{t,v} = LL_{t,v} \cdot e^{ke_L} \tag{24}$$

240 where, LLp [kg C m^{-2} day^{-1}] refers to litter production, LLl [kg C m^{-2} day^{-1}] refers to litter lost to below-ground SOM. Biomass senescence, BS_p [day^{-1}], is set to KL_p [day^{-1}] during Autumn, for deciduous plants (Table 1), LC [day^{-1}] is the fraction of litter converted to SOM each day, KT [°C] is the reference temperature and T [°C] represents the daily air temperature. Litter does not decompose if the daily temperature falls below zero. ke_L [kg C m^{-2} day^{-1}] refers to the rate of litter decomposition, adjusted by an environmental correction factor (Eq. S18, van Huissteden et al. (2006)).

2.1.5 Below-ground SOM decomposition

Peatlands consists of organic compounds at different stages of decomposition. In the model, these below-ground organic components are separated into five SOM pools (peat, humus, microbial biomass, litter & dead roots, root exudates, (Table S2). Each of the SOM pools lose and gain mass, whilst the number and the thickness of soil layers remain constant throughout the model simulation. Biodegradation of SOM leads to the mineralisation of carbon that can be reincorporated into SOM and

250 repeatedly recycled (Basile-Doelsch et al., 2020). This means that some SOM pools are active (microbial biomass, litter & dead roots, root exudates) whilst others are passive (humus, peat). Active carbon pools are available for microbial decomposition and then partitioned between CO_2 and CH_4, where, passive carbon pools decompose very slowly. Vascular plants generally have faster decomposition rates than mosses (Graf and Rochefort, 2009) and therefore vascular plants contribute to only one of the two passive SOM pools (humus, Table S2) whereas moss PFTs contribute to both passive SOM pools (humus and peat).

255 The decomposition of each SOM pool is calculated, assuming first order rate kinetics:

$$\frac{\delta}{\delta t} Q_{t,p,z,s} = -ke_{t,s} \cdot Q_{t,p,z,s} \tag{25}$$

where, SOM pools are represented by the subscript, s, Q [kg C m^{-3}] represents the mass of organic carbon in each SOM pool, ke [day^{-1}] represents the decomposition rate for each SOM pool, adjusted by an environmental correction factor (Eq. S18, van Huissteden et al. (2006)).

260 $$SD_{t,p,z} = \sum_{s=1}^{S} (ke_{t,s} \cdot Q_{t,p,z,s}) \tag{26}$$

where, SD [kg C m^{-3} day^{-1}] represents the total carbon lost from all SOM pools. A fraction of the decomposed carbon from the SOM pools (litter & dead roots, root exudates, peat) is transferred (mineralised and reincorporated) into microbial

biomass and humus, and the remaining fraction of SD is transferred into CO_2. The CO_2 flux from the decomposition of SOM is calculated, per soil layer:

$$B_{CO_2,t,p,z} = SD_{t,p,z} \cdot (1 - FMI_{p,z} - HU_{p,z}) + Rox_{t,p,z} \cdot MC \tag{27}$$

$$FMI_{p,z} = \frac{1 - HU_{p,z}}{1 + MI_{p,z}} \tag{28}$$

where, FMI [-] refers to the fraction of SOM transferred to the microbial biomass pool, calculated using PFT parameter, MI [-] (Table 1), HU [-] refers to the fraction of SOM transferred to the resistant humus pool, Rox [μM CH_4 m^{-3} day^{-1}] represents the portion of CH_4 oxidised to CO_2 (Eq. S27), and MC [kg C μM CH_4 $^{-1}$] represents the conversion factor from μM CH_4 to kg C.

2.1.6 Methane processes

The daily CH_4 flux is dependent on the production and oxidation of CH_4 as well as the three transport mechanisms (diffusion, ebullition, and plant transported CH_4). The CH_4 flux at the soil surface (Eq. 29) is calculated by summing the three transport mechanisms (diffusion, ebullition, and plant transported CH_4). The CH_4 concentration of each soil layer (Eq. S19) is calculated before summing all transport mechanisms, at the soil surface, to obtain the net flux. Methane processes were adapted from the Peatland-VU model (van Huissteden et al., 2006), originally described in Walter and Heimann (2000).

$$Ft_{t,p} = \sum_{p=1}^{P} (Fpl_{t,p}) + Fdiff_{t,z=0} + Feb_t \tag{29}$$

where, Ft [μM m^{-2} day^{-1}] represents the total daily CH_4 flux at the soil surface, Fpl [μM m^{-2} day^{-1}] represents the total plant transported CH_4 flux (Eq. 31), $Fdiff$ [μM m^{-2} day^{-1}] is the diffusive flux at the soil/water-atmosphere boundary, $z = 0$ (Eq. S20), and Feb [μM m^{-2} day^{-1}] is the ebullitive flux (Eq. S25). Methane production (Eq. S26), oxidation (Eq. S27), ebullition (Eq. S25) and diffusion of CH_4 through the soil (Eq. S20) remain as described in van Huissteden et al. (2006), originally adapted from Walter and Heimann (2000).

Plant transported CH_4 is calculated for each PFT. There are two mechanisms which determine the amount of CH_4 lost via plant transport. Firstly, the mass and distribution of the root system plays a role in determining how much CH_4 is taken up into the plant tissue. Thereby, a dense or large root system enables more CH_4 to enter the plant tissue. When CH_4 passes through the oxic zone around the root tips, a fraction of CH_4 is consumed by rhizospheric oxidation (Schipper and Reddy, 1996). This is represented by the unitless PFT parameter, $PlOx$ (Eq. 31). Secondly, the amount of CH_4 transported through the plant tissue and released to the atmosphere is determined by its aerenchyma. Plants with large aerenchyma are efficient transporters of CH_4. The PFT parameter. vP [-], describes the plant's ability to conduct CH_4 through above-ground plant tissue (Table 1). Shrubs and trees generally do not have aerenchyma whereas grasses and sedges can have large or small aerenchyma (Ström et al., 2005; Walter and Heimann, 2000). The values for these PFT parameters are taken from the literature and are cited in

Table S3.

$$Qpl_{t,p,z} = -cP \cdot vP_p \cdot LAI_{t,p} \cdot f(z,p) \cdot C_{CH_4,t,z} \tag{30}$$

where, Qpl [μM m^{-3} day^{-1}] represents the plant transported CH$_4$, cP [m^{-2} day^{-1}] is a rate constant with a value of 0.24 (taken from Walter and Heimann (2000)), $f(z,p)$ [m^{-1}] represents the exponential root distribution (Eq. 17), and C_{CH_4} [μM m^{-3}] represents the CH$_4$ concentration. The rate of plant transported CH$_4$ is integrated over the depth of the root zone to obtain the flux at the surface (Eq. 31):

$$Fpl_{t,p} = \int_{MRD}^{0} \left[Qpl_{t,p,z} \cdot (1 - PlOx_p) \right] dz \tag{31}$$

where, Fpl represents the total plant transported CH$_4$ flux [μM m^{-2} day^{-1}].

2.1.7 Harvest scheme

If the harvest scheme is activated in the model input file, PFTs taller than the prescribed harvest height are harvested (mowed) at the prescribed date. This is a relevant feature for agricultural (e.g. Knox et al. (2015)) or other managed peatlands (e.g. Evans et al. (2021)). The harvest height and days are therefore, optional prescribed model parameters. Living biomass decreases according to the amount of biomass harvested because biomass is assumed to be uniformly distributed with height and is not partitioned into organs. LAI is recalculated (Eq. 8) and the PFT height is set to the harvested height. A fixed fraction of the harvested material is assumed to be lost during the harvest process, remains uncollected in the field, and is added to the litter layer. This fraction can also be set to zero.

2.2 Two peatland sites

With this study, the PVN model simulates two peatland sites in the Netherlands, the Horstermeer site and the Ilperveld site (Fig. S1). The Ilperveld site (52°26' N, 4°56' E; 1.42 meters below sea level (mbsl)) is currently a nature recreation area that is a former raised bog complex that was drained to be used as agricultural pasture, and frequently exposed to manure fertilisation (van Geel et al., 1983; Harpenslager et al., 2015). Since the early 2000's, the Ilperveld site has undergone restoration efforts which included raising the water level, removal of the fertilised & nutrient-rich top soil, attempts to re-introduce *Sphagnum*, and water quality management. The vegetation consists of brown mosses, *Sphagnum*, and grasses (*Poaceae* family). Since restoration began, the site has been mown twice a year, in June and September. Vegetation profiles show layers of intact *Sphagnum/Carex* peat and unlike undisturbed peatlands, the top layer has undergone greater decomposition due to land management since drainage (Harpenslager et al., 2015). The Horstermeer site (52°15' N, 5°04' E; 2.1 mbsl) lies on the Horstermeer polder and is a former drained agricultural peat meadow that has not been used since the 1990s when the water level was also raised. It was used for grazing and exposed to manure fertilisation until the 1990s. The Horstermeer site is now a semi-natural fen con-

320 taining very heterogeneous vegetation, including reeds, grasses, and small shrubs, and is not subject to mowing or other land management practices (Hendriks et al., 2007). Vegetation consists of different types of grasses and sedges (dominant species *Holcus lanatus*, *Phalaris arundinacea*, *Glyceria fluitans*), and reeds (*Phragmites australis*, *Typha latifolia*). The Horstermeer polder is subject to strong seepage of mineral rich groundwater from surrounding lake areas and Pleistocene ice pushed ridges (Hendriks et al., 2007). The Horstermeer polder was a freshwater lake that was drained as part of large-scale land reclamation

325 project completed in 1888.

2.3 PFT attributes

This study defined six PFTs (*Typha*, sedges, tall grasses, short grasses, *Sphagnum*, brown mosses) based on the vegetation communities observed at the Horstermeer and Ilperveld sites. PFT attributes (Table 1) were amalgamated from the NUCOM-BOG model, the TRY 5.0 database (https://www.try-db.org, last accessed 18 May 2022) (Kattge et al., 2011, 2020) and other

330 relevant publications listed in Table S3. As much as possible, PFT parameter values are informed by observational data (i.e. Kattge et al. (2011, 2020); Heijmans et al. (2008)). Sedges, tall grasses and *Typha* all represent graminoids with deep root systems that can grow at a range of water levels but have different aerenchyma and growing ranges. Sedges are from the family *Cyperaceae* and *Juncaceae* and are grass-like, monocotyledonous flowering plants with aerenchymae. Tall grasses are from the family *Poaceae* and are grass-like plants with elongated long blade-like leaves without aerenchyma. *Typha* PFTs

335 represent a genus of about 30 species of monocotyledonous flowering plants in the family *Typhacea* with large aerenchyma. The short grasses PFT is representative of forbs and agricultural-like grasses with shallow root systems. The *Sphagnum* PFT is representative of hummock *Sphagnum* species which are generally more drought tolerant. Brown mosses represent all non-*Sphagnum* mosses but have similar but slightly broader temperature growth ranges. The SOM evolved from short grasses decomposes more easily than SOM evolved from brown mosses which decomposes more easily than SOM evolved from

340 *Sphagnum*. The six PFT input parameter sets used in this study are accessible from the bitbucket repository, bitbucket.org/ tlippmann/pvn_public.

2.4 Model calibration

The model was calibrated to reproduce fluxes that fall within the spread of observed in situ chamber measurements, measured at the Horstermeer and Ilperveld peatland sites (Sect. 2.2). The PVN model simulates processes on a daily time step. We ran

345 the model using twenty eight years (1990 - 2017, inclusive) of input data (Sect. 2.7) for the Horstermeer and Ilperveld sites. The length of the model spin-up was five years, determined by the time taken for the SOM pools, below-ground CO_2 and below-ground CH_4 concentrations to stabilise (Fig. S4). Thereby, the first five years of model simulations (1990 - 1995) are considered as the spin-up period. Daily CO_2 and CH_4 fluxes measured at the Horstermeer and Ilperveld sites between 2015 and 2017 were used to calibrate the model. Unfortunately there was not enough data to split the observational data into separate

350 datasets for calibration and validation.

A Monte Carlo analysis was performed separately for each site to calibrate thirteen model parameters (Table. S4). Parameters without available observational data were included in the model calibration process. The Kling-Gupta efficiency (KGE) metric

was used to measure the agreement between simulated and observed CO_2 and CH_4 fluxes (Gupta et al., 2009; Kling et al., 2012). The KGE approach is a three dimensional decomposition of the Nash-Sutcliffe efficiency (NSE) measure and evaluates temporal dynamics, bias, and variability Eq. 28. The KGE metric has been used to assess the ability of carbon flux models (Tramontana et al., 2016; Zhao et al., 2020), hydrological models (Dick et al., 2015), and meteorological reanalysis datasets (Chaney et al., 2014; Muñoz-Sabater et al., 2021) to reproduce in situ observations. The calibrated model input values are provided in Table S6 and Table S7 for the Horstermeer and Ilperveld site simulations, respectively.

The CO_2 results impact the CH_4 results much more than the CH_4 results impact the CO_2 results, therefore we first ensured that the parameters impacting the photosynthesis, and above and below ground growth and respiration schemes reproduced fluxes that fell within the spread of observed CO_2 fluxes (NEE). These were the MolAct, HalfSatPoint, VegTScalingFactor parameters. Next, the CH_4 scheme was calibrated to reproduce fluxes that fell within the spread of observed CH_4 fluxes. This involved calibrating the remainder of the parameters highlighted in Table. S4. Even though the amount of photosynthesis and living biomass does not directly impact the CH_4 production, which primarily occurs in the soil and above-ground litter layers, these processes are precursors to root and shoot growth, respiration, and senescence, which directly impact simulated CH_4 fluxes. After optimisation of the CH_4 fluxes, the PFT parameters (Table S3) were manually adjusted to bring the PFT biomass fractions (PFT biomass as a fraction of total biomass) in line with observed aerial cover fraction ratios. The calibrated model parameters and the necessary input files used to simulate the two peatland sites evaluated in this study are accessible from the bitbucket repository, bitbucket.org/tlippmann/pvn_public.

2.5 Testing the PVN model

To understand the sensitivity of net CO_2 and CH_4 fluxes to PFT dependent processes, we conducted several model simulations using modified input data. Air temperature, water table, radiation, harvest, and the swapping of PFTs between site simulations were chosen to be used for the sensitivity testing because they are key environmental drivers of CO_2 and CH_4 emissions in peatlands. We tested the sensitivity of PFTs processes by varying these inputs one by one (Table 2).

Table 2. A summary of the varied input data used to understand the sensitivity of the model. *To compare the PFT dynamics, both simulations use the 'no harvest' regime. The exchange of PFTs means that the model simulation driven by the Ilperveld input data (Table 4) will use the PFTs observed at the Horstermeer site (*Typha*, tall grass, sedges, brown moss PFTs) while the model simulation driven by the Horstermeer input data will use the PFTs observed at the Ilperveld site (short grass, tall grass, *Sphagnum*, brown moss PFTs).

Changing input variable	Input change
Air temperature	$\pm 1\,^\circ$C, $\pm 3\,^\circ$C
Harvest frequency	no harvest; once, twice, three, and four times per year
PFTs	Exchange Ilperveld and Horstermeer PFTs*
Radiation	± 8 J m^{-2}, $+100$ J m^{-2}, $+200$ J m^{-2}
Water level	± 0.1m, ± 0.2m

To understand how the new model mechanisms affect emissions, we performed additional simulations with altered model algorithms and compared these to the original model simulations calibrated for the Horstermeer and Ilperveld sites (Table 3).

Table 3. A summary of the simulations with altered model algorithms.

Simulation name	Mechanism change
CH4_OLD_CF	Uses Peatland-VU CH_4 module multiplied by the PFT cover fraction
CF_CONST	Biomass fraction is constant for all PFTs, i.e. BF = 0.25
FPAR_CONST	FPAR is constant for all PFTs, i.e. FPAR = 0.25
HEIGHT_CONST	Constant plant height for each PFT

For example, the contribution of competition for shading to the overall simulation result, is quantified by comparing an altered simulation where incoming photosynthetically active radiation (PAR) is independent of shading (e.g. fractional par or FPAR = 0.25 for a simulation with four PFTs) to the original model simulations (FPAR_CONST). We calculated the relative difference of the simulation with shading minus the simulation without shading. Similarly, we compared simulations with and without plant transported CH_4 (CH4_OLD_CF), with and without dynamic BF (CF_CONST), with and without variable plant height (HEIGHT_CONST).

In order to demonstrate that the PVN model reproduces CH_4 and CO_2 fluxes within the spread of observed fluxes when driven by realistic input data, we compared the calibrated model simulation results and measured CH_4 and CO_2 fluxes for the Horstermeer and the Ilperveld field sites (Sect. 2.2).

We compare the CH_4 and CO_2 fluxes of the calibrated model simulation results against the CH_4 and CO_2 fluxes simulated by the Peatland-VU model to understand the impact of introducing PFTs on the simulation of CH_4 and CO_2 fluxes. These model simulations are summarised in Table 4. Attempts to run the Peatland-VU model with new calibrated parameters did not yield results in the same order of magnitude as the observations. Therefore, it was necessary to use different model parameterisations for the PVN and Peatland-VU models.

2.6 Flux measurements

Carbon dioxide and CH_4 fluxes were measured using 2-4 automated flux chambers (AC) and the Ultra-Portable Los Gatos Gas Analyser Model 915-001. Chambers were cylindrical, 30cm wide and 40cm in height, made of transparent acrylate, equipped with a fan and installed in the field using collars. Where necessary, vegetation was folded gently to fit inside the measurement chambers. Collars were removed from the field between sampling campaigns which minimises disturbance which can lead to potential biases in the observations. This also potentially introduces uncertainty as to the precise measurement location. The CO_2 and CH_4 concentrations were measured for 150 second intervals, whilst the chamber was closed. Each chamber was measured on rotation so that a new chamber was measured every 15 minutes. Measurements were recorded continuously, during the day and night, for a week at a time, upon which the AC system was moved to another site. We note that due to the labor intensive nature of accumulating chamber observations consistently through time, these observational datasets do not offer complete temporal continuity, creating an intermittency bias. From this data, the hourly average CO_2 (net ecosystem exchange) and CH_4 fluxes were calculated for each day. We compared calibrated site simulations against observed daily average CO_2 and CH_4 fluxes. To visualise the daily variability, standard deviations were derived from the hourly fluxes. The values for

17

all GHG emissions are expressed as CO_2 equivalents ($kgCO_{2eq}m^{-2}yr^{-1}$) and calculated as

405 $$GHG_{CO_2e} = CH_4 \cdot GWP + CO_2 \qquad\qquad\qquad (32)$$

where,

$GWP_{20} = 80.8$, as 1 $kgCH_4$ = 80.8kg CO_2eq, over a 20 year time horizon, and

$GWP_{100} = 27.2$, as 1 $kgCH_4$ = 27.2 kg CO_2eq, over a 100 year time horizon (Masson-Delmotte et al., 2021).

2.7 Input data preparation

410 The PVN model is driven by daily air temperature (T), water level (WL), radiation, a general model parameter input file (Table. S4), and a soil parameter input file (Table S5).

2.7.1 Climatological input data

Daily temperature and radiation data, measured at Schiphol, the nearest KNMI weather station was used as climate input data for both sites (accessed via https://www.knmi.nl/nederland-nu/klimatologie/daggegevens, last accessed 18 May 2022) (Fig.
415 S3). The annual average rainfall at Schiphol, was 850 mm yr^{-1} over the period, 1990-2020, with 30% of the rainfall falling in summer and autumn, respectively, and 24% falling in winter, with the remainder falling in the spring. The average daily temperature between 1990 and 2019 was 9.4 °C and warmed approximately +0.1 °Cyr^{-1} over the same period. The average daily temperature for the warmest month, August, was 22.1 °C and the lowest daily monthly temperature for the coldest month, January, was 0.8 °C.

420 #### 2.7.2 Soil profile input data

The model generates a soil horizon representation using soil layers of 10cm thicknesses. The generated soil horizon uses properties such as dry bulk density (DBD), SOM ratio, sand content, C:N ratio specified in the soil profile input data (Table S5). The number and depth of the site's soil horizons can be adjusted in the soil input file. The PVN model requires input parameters for each PFT, discussed in Section 2.3. Soil profile data from the Horstermeer and Ilperveld field sites was collected
425 in 2015 and 2016 and includes DBD, C content, SOM content, sand and clay content, pF curve (Table S8 and Table S9, for the Horstermeer and Ilperveld site simulations, respectively).

2.7.3 Water level input data

Water level input data was sourced from the Dutch hydrological model, Netherlands Hydrological Instrument (NHI) (De Lange et al., 2014), which has a reasonably high spatial resolution (250m x 250m). One aim of developing the PVN model is
430 to eventually develop a model of all Dutch peatlands in conjunction with the NHI product. For this reason, the NHI product is used in this application of the model. The NHI water level output was converted to relative surface height using a 5m x 5m digital elevation map of the Netherlands, Actueel Hoogtebestand Nederland (Alhoz et al., 2020). It is possible to use in situ

Table 4. A summary of the model simulations, using both the new PVN model and the pre-existing Peatland-VU (PV) model. Model input parameters for the Horstermeer and Ilperveld site simulations are provided in Table S6 and Table S7, respectively.

Site	Model	Vegetation	Harvest height
Horstermeer	PVN	*Typha*, sedges, tall grass, brown moss	-
Horstermeer	PV	-	-
Ilperveld	PVN	Short grass, tall grass, brown moss, *Sphagnum*	0.15m
Ilperveld	PV	-	0.15m

water levels as input data for the model but this data was unfortunately, unavailable for the duration of the simulation. The input data used for both sites is accessible from the bitbucket repository, bitbucket.org/tlippmann/pvn_public.

3 Results

When describing the annual CO_2, CH_4, and GHG values, we opt to use the term emissions, e.g. 'annual GHG emissions', whereas, when describing daily values, we opt to refer to these as fluxes, e.g. 'daily GHG fluxes'.

3.1 Model sensitivity to input data

To understand the response of the modeled PFT processes to input data, we ran simulations with modified water levels (Fig. 3 and Fig. S6), temperature (Fig. 2 and Fig. S5), radiation (Fig. S7) input and harvest schemes (Fig. 4). The modified input data is summarised in Table 2 and the results of these sensitivity tests are summarised in Table 5. These results are indicative of the model's mechanistic responses rather than projections on how PFTs might respond under varied environmental conditions. To show how different inputs impact model processes, we present the soil (respiration) CO_2 emissions (Fig. 3), plant transported CH_4 (Fig. 2), and above-ground biomass (Fig. 4). In the PVN model, the abundance of each PFT varies through time depending on the favourability of growing conditions. Therefore, an increase in CO_2 or CH_4 emissions may be due to increased abundance (i.e. enhanced biomass) or enhanced transport efficiency. To disentangle this difference, the CO_2 and CH_4 emissions for each PFT are plotted as a fraction of litter and root mass.

Increased air temperatures had a positive effect on both plant transported CH_4 emissions (Fig. 2) and litter & root mass at both sites (Fig. S5). Short and tall grasses showed similar responses to increased air temperatures by producing large CH_4 emissions per kg of litter and root mass. Brown mosses showed little variation between the temperature experiments for the Ilperveld site but showed a decrease in emissions with warming temperatures per kg of litter and root mass at the Horstermeer site. *Sphagnum* similarly showed a decrease in CH_4 emissions with warming temperatures per kg of litter and root mass at the Ilperveld site. This decrease is because moss PFTs have strict ideal temperature growth limits (T_{max} and T_{min} in Table 1) and were limited by warming temperatures. Whilst below-ground CH_4 concentrations increased with warming temperatures, the biomass, litter, and root mass of moss PFTs did not increase with warming temperatures.

Below-ground CO_2 emissions were impacted by changing water levels (Fig. S6). Previous studies have found that below-ground CO_2 production tends to increase with low water levels due to enhanced potential for aerobic CO_2 production (Knox

19

Table 5. The results of the sensitivity testing. The CH_4 and CO_2 columns indicate how much the respective emissions changed when the input changed, relative to the results of the respective default Horstermeer and Ilperveld PVN simulations described in Table 4. A dash [-] indicates the simulation is the default site simulation. An overview of the sensitivity tests can be found in 2.

Changing input variable	Input change	Horstermeer		Ilperveld	
		CH_4 [%]	CO_2 [%]	CH_4 [%]	CO_2 [%]
Air temperature	+3°C	165	117	115	122
	+1°C	128	94	102	108
	-1°C	77	93	100	87
	-3°C	56	66	154	53
Harvest frequency	no harvest	-	-	120	129
	1 year^{-1}	114	68	87	117
	2 year^{-1}	114	67	-	-
	3 year^{-1}	115	67	152	70
	4 year^{-1}	114	68	185	45
PFTs	*Typha*, sedges, tall grass, brown moss	-	-	291	294
	Short grass, tall grass, brown moss, *Sphagnum*	35	68	-	-
Radiation	+200 J m^{-2}	121	107	97	126
	+100 J m^{-2}	111	104	98	113
	+8 J m^{-2}	101	101	98	101
	-8 J m^{-2}	99	99	98	99
Water level	+0.2m	149	104	200	99
	+0.1m	134	103	172	100
	-0.1m	98	98	87	101
	-0.2m	163	97	281	101

et al., 2015). The results of the Ilperveld site sensitivity simulations showed that below-ground CO_2 production increased with low water levels, likely due to enhanced potential for aerobic CO_2 production. However, the results of the Horstermeer site sensitivity simulations showed the converse, that the net CO_2 (Table 5) and below-ground CO_2 production increased with high water levels. We simulate that with high water levels, the reduced aerobic CO_2 production can be exceeded by the enhanced oxidation of CH_4 into CO_2. The large amounts of CH_4 oxidised into CO_2 in the Horstermeer site simulation are due to the very degraded peat present at the site (represented by low soil OM content in the soil input file) and the strong upwelling of rich groundwater at the Horstermeer site (represented by the calibratable model parameter, MolAct (see Sect. 2.4), which influences the sensitivity of aerobic CO_2 production). The large observed CH_4 emissions at the Horstermeer site are partially due to high CH_4 concentrations in the upwelling water. Furthermore, the large root systems of plants such as *Typha*, sedges and tall grasses have greater potential to access and transport stores of below-ground gases (represented by the PFT root depth
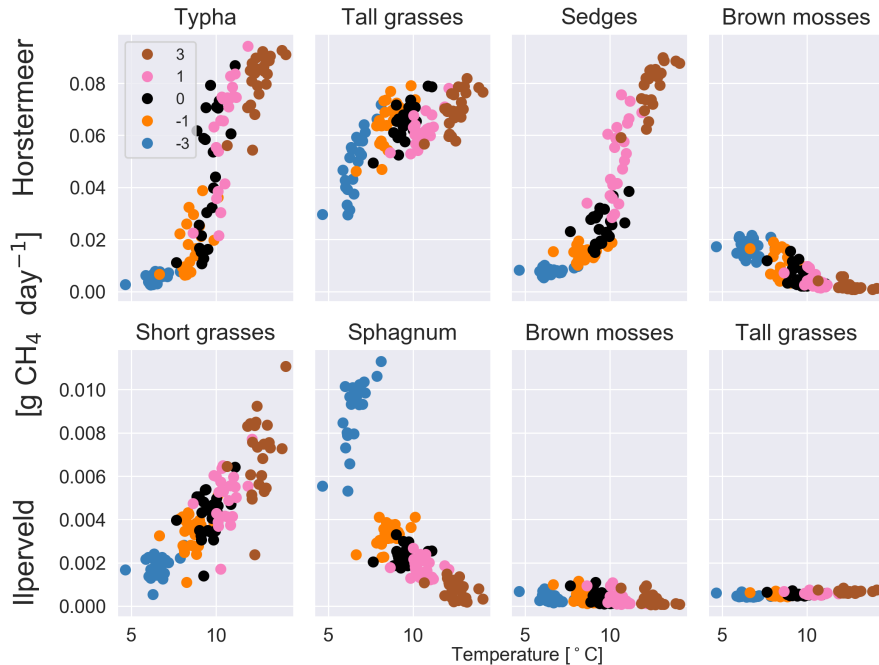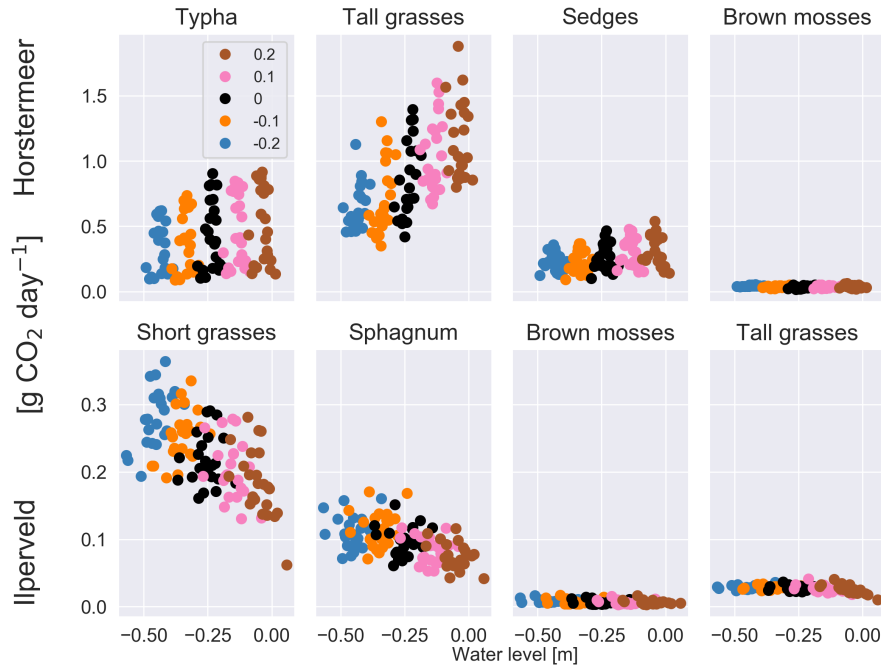
Figure 2. The results of the sensitivity tests show the relationship between different temperature inputs and the mean daily plant transported CH_4 for each year, for each of the PFTs at the Horstermeer site (top row) and Ilperveld site (bottom row). Temperature input was increased and decreased by 1 & 3 °C, respectively. The legend shows the input change in °C where, $\pm$ signs in front of the legend labels show the direction of change. Note the different y axes between the top and bottom panels.

and mass). The conflicting response of the tall grass PFT in the Ilperveld and Horstermeer simulations shows that PFTs may respond differently to changing water levels at different sites.

470　　Increasing the frequency of harvests led to a strong negative effect on vascular plant biomass and a small positive effect on moss plant biomass (Fig. 4). Biomass of non-moss PFTs is strongly impacted by the occurrence of harvests as indicated by the pause in biomass accumulation after harvest. However, by reducing tall vegetation, moss species have greater access to sunlight and therefore, gain an advantage. For this reason, we saw the biomass of moss PFTs increase with more frequent harvests. In the Horstermeer site simulation, the greatest effect on biomass was between no harvests and the once per year harvests. In

475　the Ilperveld site simulation, the effects of harvests on biomass increased somewhat linearly, according to the frequency of harvest events. We suspect that this is due to the inclusion of different PFTs in the two site simulations. In the Horstermeer site simulation, three PFTs have the capacity to grow above the harvest height (the *Typha*, tall grass, and sedge PFTs) whereas in the Ilperveld site simulation only tall and short grasses have the potential to grow beyond the harvest height, thereby limiting the potential effect harvests can have on the PFTs present. Furthermore, the growth of the short grasses PFT is height limited

480　to 0.3m. Overall, total biomass was reduced with more frequent harvest regimes.

It's important to note that whilst CO_2 emissions reduced by increasing the frequency of harvests, these emissions are not accounting for the off-site decomposition of harvested biomass. Methane emissions were slightly enhanced if harvests occurred,

21

Figure 3. The results of the sensitivity tests show the relationship between different water level inputs and the mean daily soil CO_2 flux for each year, for each of the PFTs at the Horstermeer site (top row) and Ilperveld site (bottom row). Water level input was decreased by 0.1 & 0.2 m and increased by 0.1 & 0.2 m, respectively. The legend shows the input change, where $\pm$ signs in front of the legend labels indicate the direction of change. Note the different y axes between the top and bottom panels.

in comparison to no harvest events, for Horstermeer site simulations, whilst the frequency of harvests did not impact emissions (Table 5). Similarly, enhanced CH_4 emissions occurred with increased harvest frequency for Ilperveld site simulations. Spikes in CH_4 fluxes transported by vascular PFTs occurred after harvest events in both the Horstermeer and Ilperveld simulation results (not shown), contributing to enhanced CH_4 emissions, for both Ilperveld and Horstermeer site simulations. The impact of fewer or no harvest events led to variable impacts on CH_4 emissions for Ilperveld site simulations, where a single harvest led to slightly reduced emissions and no harvests led to slightly enhanced emissions. In the Ilperveld site simulation without harvest events, vegetation became dominated by vascular PFTs that are efficient transporters of CH_4, leading to enhanced CH_4 emissions.

## 3.2 Assessment of model mechanisms

To understand the role of isolated model mechanisms, we modified the model code to disable the functions responsible for reproducing the vegetation dynamics within in the model (Fig. 5). Unlike the other simulations assessed throughout this paper, the simulation results shown in Fig. 5 begin in the year 1990. i.e. without the use of a spin up period. Removing the spin up period showed that the modified model simulation results produce similar emissions in the first year of the simulation (1990) and allows assessment of the trajectory of deviation.
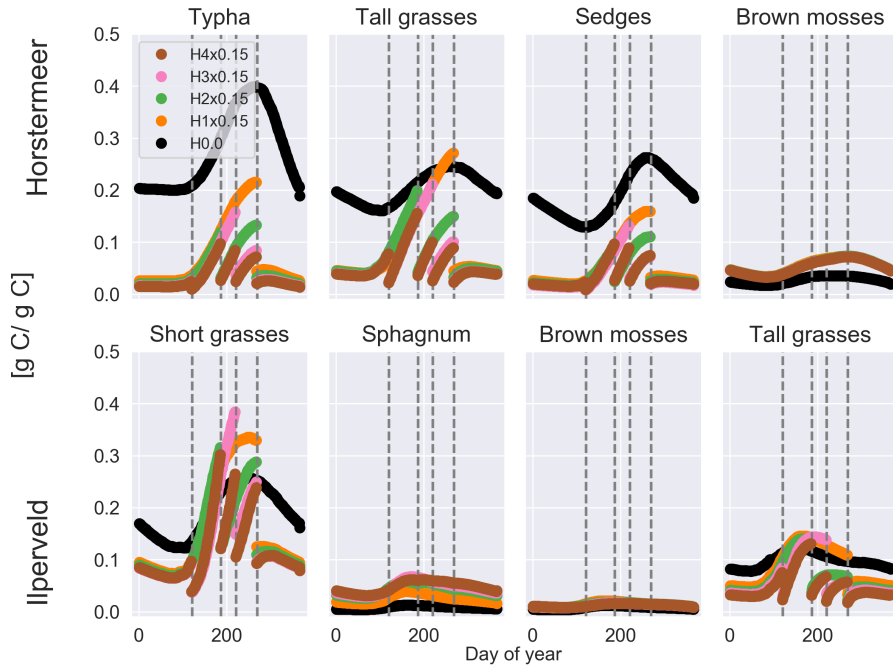
Figure 4. The results of the sensitivity tests show the relationship between different harvest schemes and biomass for each day of year (shown as a fraction of litter & root mass) at the Horstermeer site (top row) and Ilperveld site (bottom row). Vegetation is cut to 0.15m (x0.15) at the moment of harvest. The legend shows the harvest input scheme and the vertical dotted lines indicate the four possible harvest days (days 120, 186, 220 and 268). Harvest was set to either not occur (H0.0), occur once per year (H1x0.15) on day 268, twice per year (H2x0.15) on days 186 and 268, three times per year (H3x0.15) on days 120, 220 and 268, or four times per year (H4x0.15) on all harvest days.

Disabling the shading scheme (simulation PVN_HEIGHT_CONST) or biomass fraction scheme (simulation PVN_CF_CONST) led to only slightly enhanced CO_2 emissions, whereas disabling the FPAR scheme (simulation PVN_FPAR_CONST) led to large CO_2 emission differences. Surprisingly, the difference for the PVN_FPAR_CONST simulation is opposite in sign for the two site simulations, and larger for the Ilperveld simulation. This means that maintaining constant FPAR, led to a small enhancement of CO_2 emissions in the Horstermeer simulation but a large reduction of CO_2 emissions for the Ilperveld simulation. These results show that FPAR plays a large role on simulated CO_2 emissions. The results of Ilperveld PVN_FPAR_CONST simulation results also showed that the FPAR function has the potential to introduce large variability into the emission results. This is interesting to note because the PVN model showed limited skill reproducing the CO_2 emissions at the Ilperveld site. These results indicate that the function calculating FPAR plays a driving role on CO_2 emissions but particularly at the Ilperveld site. Further model developments may investigate ways to improve the representation of FPAR in the model. The PVN_FPAR_CONST simulations also led to enhanced CH_4 emissions for the Ilperveld simulation. It is likely that CH_4 production was enhanced due to increased stores of CO_2.

The use of the Peatland-VU CH_4 scheme (PVN_CH4_OLD_CF) led to large differences in CH_4 emissions for both the Horstermeer and Ilperveld simulations, in comparison to the PVN model results. The CH_4 emissions of the model simulations
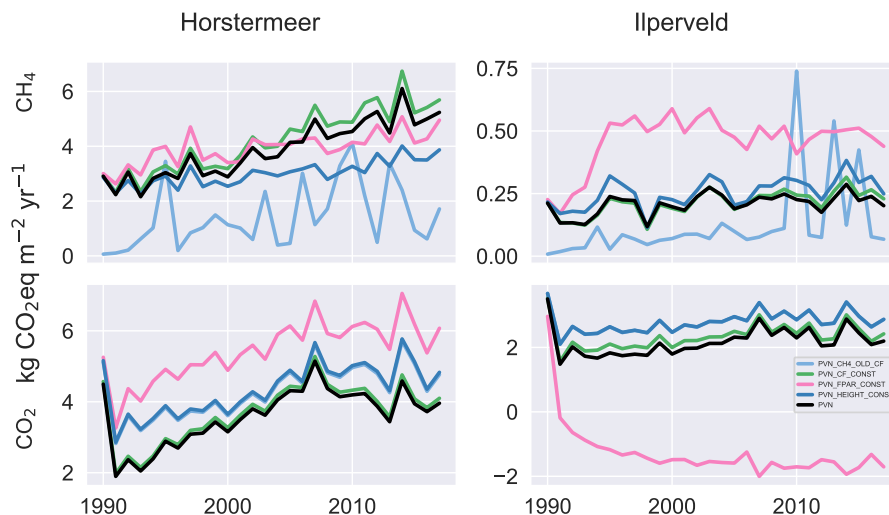
Figure 5. The CH_4 and CO_2 emissions for various isolated model mechanisms, compared against the PVN model result. We investigated maintaining constant fractional PAR (PVN_FPAR_CONST), maintaining constant plant height (PVN_HEIGHT_CONST), maintaining constant cover fraction (PVN_CF_CONST), and including the original Peatland-VU CH_4 module multiplied by the PFT cover fraction (PVN_CH4_OLD_CF), at each time step.

that use the Peatland-VU CH_4 scheme (simulation PVN_CH4_OLD_CF) were small when compared to the CH_4 emissions of the PVN model, for both model simulations. This indicates that the PFT modifications to the CH_4 scheme have led to substantial impacts on modeled CH_4 emissions.

3.3 Assessment of calibrated model simulations

515 Here, we describe the simulation results of the model calibrated at two field sites, the Horstermeer and Ilperveld. We describe the net annual CH_4 and CO_2 emissions, and GHG budgets (Fig. 6), as well as simulated PFT dynamics as indicated by changes to LAI, above-ground biomass, litter mass, and PFT height/depth (Fig. 7 and Fig. S8). All net GHG values are expressed as CO_2 equivalents (CO_{2eq}). The model simulation results indicate that the simulated annual mean net GHG emissions from the Ilperveld simulation were approximately half the emissions of the Horstermeer simulation. However, these model emission

520 estimates are not considering off-site decomposition of harvested biomass. The model estimated that the 2015-2017 annual average net GHG emissions were 2.5 and 8.9 $\mathrm{kgCO_{2eq}m^{-2}yr^{-1}}$ for the Ilperveld and Horstermeer simulations, respectively (Table 6), calculated using the 20 year GWP. Using the 100 year GWP, the 2015-2017 annual average net GHG emissions were 2.3 and 5.6 $\mathrm{kgCO_{2eq}m^{-2}yr^{-1}}$ for the Ilperveld and Horstermeer simulations, respectively. The model estimated that the 1995-2017 annual average net GHG emissions were 2.4 and 8.0 $\mathrm{kgCO_{2eq}m^{-2}yr^{-1}}$ for the Ilperveld and Horstermeer model

525 simulation results, respectively (Fig. 6), calculated using the 20 year GWP. Using the 100 year GWP, the 1995-2017 annual average net GHG emissions were estimated to be 2.3 and 5.2 $\mathrm{kgCO_{2eq}m^{-2}yr^{-1}}$ for the Ilperveld and Horstermeer model simulation results, respectively. Assessment of the Horstermeer simulation showed that on average, CH_4 contributed approximately
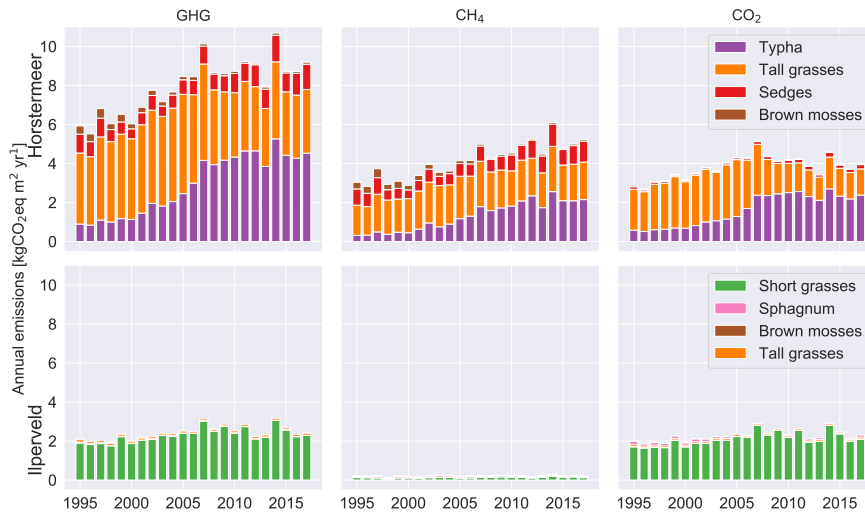
Figure 6. Relative contributions of each PFT to simulated annual average net GHG (left), CH_4 (middle), and CO_2 (right) emissions. The results of the Horstermeer site simulation are represented in the top row and the results of the Ilperveld site simulation are represented in the bottom row.

half (52%) of the net annual GHG emissions of the Horstermeer simulation, where CH_4 contributed 4.2 $kgCO_{2eq}m^{-2}yr^{-1}$ and CO_2 emissions contributed 3.8 $kgCO_{2eq}m^{-2}yr^{-1}$, on average. Assessment of the Ilperveld simulation showed that CO_2

530 was the primary contributor to net GHG emissions, where CO_2 contributed the majority (92%) of the annual GHG emissions (2.2 $kgCO_{2eq}m^{-2}yr^{-1}$ of the total 2.4 $kgCO_{2eq}m^{-2}yr^{-1}$ net GHG emissions). These model emission estimates neglect the off-site decomposition of harvested biomass. Therefore, CO_2 and CH_4 emissions are equally contributing to the net GHG emissions in the Horstermeer simulation, whereas, CO_2 emissions dominate the GHG emissions in the Ilperveld simulation results.

535 To assess whether there was an increasing or decreasing trend in emissions over the duration of the simulation (1995-2017), we calculated the linear regression of the CO_2, CH_4, and net GHG time series of the simulation results at both sites. The trend of Horstermeer simulation emission results was 0.13, 0.06, and 0.19 $kgCO_{2eq}m^{-2}yr^{-1}$ for CH_4, CO_2, and the net GHG emissions. Daily temperature observations show local temperatures increased by +0.1C $°Cyr^{-1}$ between 2010 and 2017, or +0.06 $°Cyr^{-1}$ over the entire simulation period (1995-2017). The trend results for the Ilperveld simulation emissions were zero

540 for CH_4 emissions, and 0.04 $kgCO_{2eq}m^{-2}yr^{-1}$ for CO_2 and net GHG emissions. Warming temperatures are a possible driver of the enhanced GHG emissions at the Horstermeer site. The increase in GHG emissions of the Horstermeer site simulation and the little or no increase of the Ilperveld site simulation are aligned with the results of the +1°C temperature sensitivity tests. The results of the Horstermeer site sensitivity tests showed that the *Typha* and sedge PFTs were sensitive to warming temperatures, and therefore the increase in the biomass and GHG emissions of the *Typha* and sedge PFTs at the Horstermeer

545 site are likely due to enhanced temperatures.

25

3.3.1 PFT dynamics

Here we describe the living biomass, LAI, litter layer, biomass fraction, and height changes of the PFTs of the calibrated Horstermeer and Ilperveld model simulations (Fig. 7 and Fig. S8). Assessment of above-ground biomass (top row of Fig. 7) shows that the tall grass (blue line), *Typha*, and sedge PFTs (red line), were abundant during the Horstermeer simulation whereas the Ilperveld simulation was dominated by the short grass (green line), *Sphagnum* (pink line) and tall grass PFT (blue line). All plants showed seasonal variability. The ratio of the litter layer to biomass, is between approximately 1:4 and 1:3 for most PFTs (kg C). The *Typha* PFT is an exception, and the ratio is approximately 1:1. Overall, the sedge PFT showed comparable seasonal variability to the tall grass PFT whilst maintaining less biomass, smaller LAI, and shorter height throughout the Horstermeer simulation. The similar behaviour of the *Typha*, sedge, and tall grass PFTs was expected because the PFT input parameters represent similar plant phenologies. Assessment of the size of the litter layer (first row of Fig. S8) showed that in the Ilperveld simulation, the PFTs reached peak litter during Autumn (September) whilst in the Horstermeer simulation which is not mown, the litter continued to accumulate until January where rates of decomposition exceeded accumulation. The LAI (second row of Fig. S8) displayed strong seasonal variability. Each year, the LAI of the Short grasses reaches its maximum LAI value of 1.2. The tall grass PFT, whilst very competitive in the Horstermeer simulation is less competitive in the Ilperveld simulation, partially due to the occurrence of harvests and partially because it is out-competed by the fast growing short grass PFT. Assessment of the Ilperveld simulation reveals that the short grass PFTs were constrained by the maximum height parameter, MaxCanopyHeight. The tall grass PFT was not limited by MaxCanopyHeight in the Ilperveld simulation but was instead limited by the biannual mowing regime. PFT height showed strong seasonal variability for both simulations (third row of Fig. S8). The tall grass PFT was the tallest plants in the Horstermeer simulation until 2009 and its height was frequently limited by the PFT MaxCanopyHeight parameter. However, as the *Typha* PFT grew in biomass, the tall grass PFT appeared to have less access to sunlight as height and biomass values reduced. The *Typha* and sedge PFTs were not limited by their maximum height parameters. These changes in biomass fraction are also evident in the emissions.

The relative contributions of each PFT towards the net annual CH_4, CO_2, and GHG emissions are shown in Fig. 6 where the CH_4 emissions refer to only the plant transported CH_4. The net CO_2 emissions for each PFT are the sum of the photosynthesis minus respiration, the CO_2 produced by below-ground aerobic decomposition of SOM, and a portion of CH_4 oxidised to CO_2. The tall grass (red boxes), sedge (orange boxes), and *Typha* (purple boxes) PFTs are large transporters of CH_4 emissions of the Horstermeer simulations results. However, only the tall grasses and *Typha* compose the net CO_2 emissions in the Horstermeer simulation. Thereby, the tall grass PFT was the largest contributor to the net annual GHG emissions, followed by the *Typha* and sedges PFTs. The Ilperveld simulation results showed that the short grass PFT was the largest contributor to the net annual CH_4, CO_2, and GHG emissions.

3.4 Comparison of modelled and observed plant dynamics

We compare simulated PFT biomass fractions against observed aerial plant cover fractions (Fig. 8). For assessment against observational data we compare model simulation results against observed fluxes by comparing time series, box plots, and 1:1
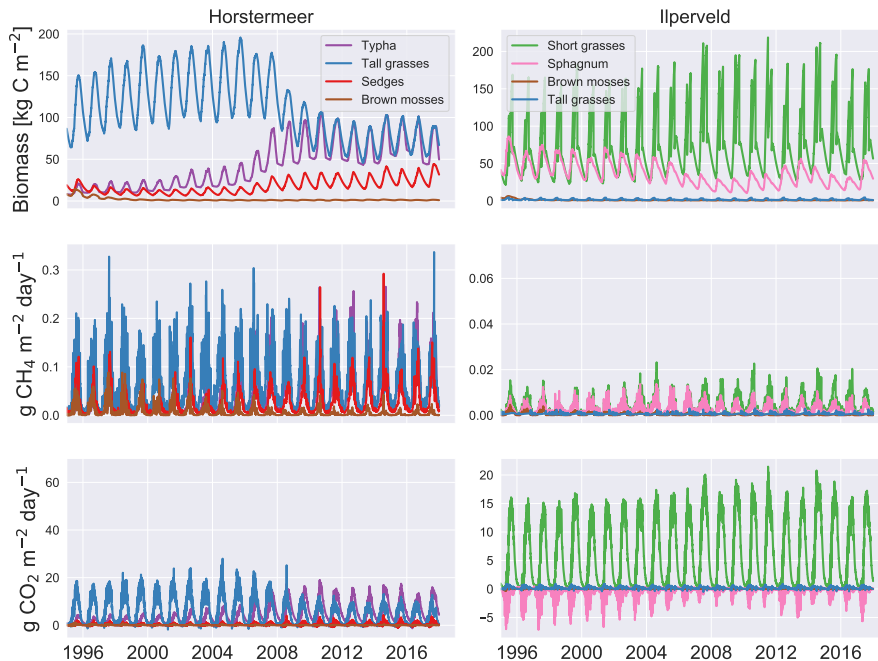
Figure 7. Vegetation dynamics. The results of the Horstermeer site simulation are represented in the left column and the results of the Ilperveld site simulation are represented in the right column. Note the differing y axes.

scatter plots for CH_4 (Fig. 9) and CO_2 (Fig. 10). Gaps in observational data exist due to measurement collection limitations, and therefore the model comparison against observational data can only be shown for the days where observational data exist. Unfortunately, this means that the model was not assessed equally across all seasons or, on the same days of the year at the two sites. A simple linear regression is used to compare the model simulation results and observational data using all days with available measurements. For these reasons, the 1:1 plots, and R^2 linear regression results may only give a flavor of model performance. To understand the degree of uncertainty of the observational measurements, daily standard deviations were derived using the hourly fluxes (plotted as black error bars in Fig. 9 and Fig. 10). In each case the model simulation results generally lay within the spread of observational uncertainty. The observations indicated that both sites are annual sources of CH_4 and CO_2, and therefore, net annual sources of carbon to the atmosphere. The Horstermeer site (purple line in Fig. 9) and CO_2 (Fig. 10) produced large annual mean CH_4 and CO_2 emissions in comparison to the Ilperveld site (green line in Fig. 9) and CO_2 (Fig. 10).

3.4.1 Evaluation of plant composition dynamics

Plant cover fraction observations were made at the location of the chamber measurements and were not representative of the site's plant complete community composition. Although aerial cover fraction and biomass fraction (the ratio of PFT biomass to total biomass) are not the same, changes in plant composition are depicted in both representations.

27
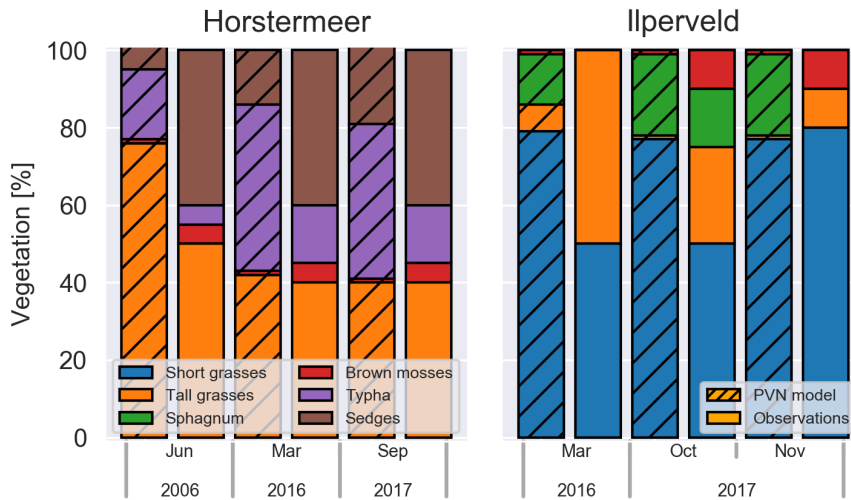
Figure 8. Simulated PFT biomass fractions and observed areal cover fractions at Horstermeer (left) and Ilperveld (right).

In 2006, the chamber measurement location at the Hostermeer field site was composed of tall grasses (50%), sedges (40%),

595   *Typha* (5%), and brown mosses (5%) (left panel in Fig. 8). The Horstermeer simulation results have good agreement with the observations but overestimated the amount of tall grasses (66%) and underestimated the amount of Sedges (40%). In 2016, a decade later, the amount of tall grasses remained consistent, whilst the amount of *Typha* had increased by 10%. One year later in 2017, the vegetation had not undergone changes, proportionally. Parallel to the observations, the Horstermeer simulation results estimated that the tall grass PFTs decreased to 60%, from 2005 onwards whilst, the biomass fractions of the *Typha*

600   and sedge PFTs increased. Overall, the Horstermeer simulation overestimated the biomass fraction of the tall grass PFT, and underestimated the proportion of the sedges and *Typha* PFTs. Model estimates of year-to-year PFT biomass changes were of the same sign and similar magnitude as in situ observations.

In March 2016, the chamber measurement location at the Ilperveld field site hosted short grasses (50%) and tall grasses (50%). The model overestimated the amount of short grasses (80%), underestimated the amount of Tall grasses (5%), and

605   overestimated the amount of *Sphagnum* (10%). The *Omhoog met het Veen* (Raising the Peat) project delivered onsite managements attempts to initiate *Sphagnum* growth by hand dispersing living fragments of *Sphagnum spp.* from a nearby donor site between 2013 and 2015 (Geurts and Fritz, 2018). For this reason, we expected that the model may not match the development of *Sphagnum* at the Ilperveld site. In October 2017, the vegetation shifted to be composed of short grasses (50%), and tall grasses (25%), *Sphagnum* (15%), and brown mosses (10%). One month later in November 2017, the *Sphagnum* was no longer

610   visible (0%), brown mosses remained (10%), and the site was dominated by short grasses (80%). The model estimated that the short grass and *Sphagnum* PFTs remained consistent into 2016 and 2017, whilst the tall grass PFT reduced and brown mosses increased slightly. Whilst the model simulations ended in 2017, we saw that in October 2018, the vegetation remained constant at both sites.

28

3.4.2 Evaluation of simulated CH$_4$ fluxes

The time series presented in Fig. 9 shows the behaviour of the Horstermeer simulation CH$_4$ flux results (purple line), the observed mean daily fluxes (black dots) and the spread of the hourly observed fluxes (black error bars). Whilst the Horstermeer simulation reproduced the seasonal variability of the observed CH$_4$ fluxes, the box plots showed that the simulation results (purple box) tended to overestimate the CH$_4$ fluxes. Overall, the Horstermeer simulation showed a robust pattern of variability when compared with the observations (R^2 = 0.7) whilst overestimating the magnitude of observed fluxes. Assessment of the Ilperveld model simulation showed that the model was able to reproduce the observed CH$_4$ fluxes and followed the pattern of variability when compared with the observations (R^2 = 0.8). The summer of 2015 is an exception where the simulated results showed an increase in CH$_4$ fluxes, larger than the observed CH$_4$ fluxes. Assessment of the box plots showed that the simulated CH$_4$ fluxes (green box) are of similar mean and spread to the observed fluxes (purple box).

3.4.3 Evaluation of simulated CO$_2$ fluxes

The box plots showed that the PVN Horstermeer simulation reproduced the median and range of observed daily CO$_2$ fluxes at the Horstermeer site. The results of the Horstermeer site simulation (purple line) reproduced the 2015, 2016, 2017 Spring CO$_2$ fluxes. The results of the Horstermeer site simulation captured the 2015 and 2016 Autumn fluxes. However, the model generally overestimated the magnitude of simulated fluxes (purple box) but generally reproduced the variability (R^2 = 0.8).

The box plots in Fig. 10 showed that the Ilperveld simulation results (green box) generally overestimated CO$_2$ fluxes. The box plots showed that the mean hourly CO$_2$ flux simulated by the model was a small positive flux, 250 $\mathrm{mgCO_2m^{-2}hr^{-1}}$ whereas the observed mean hourly flux was 0 $\mathrm{mgCO_2m^{-2}hr^{-1}}$. The Ilperveld simulation (green line) captured the early spring fluxes in 2016, and 2017. However, during 2015 and 2016, the model tended to overestimate the observed CO$_2$ fluxes. Comparison of the simulated daily hourly average (green line) and the spread of hourly fluxes (black error bars) showed that the simulated CO$_2$ fluxes (green line) fell within the spread of daily hourly fluxes. The model showed some agreement with the observed pattern of variability (R^2 = 0.6).
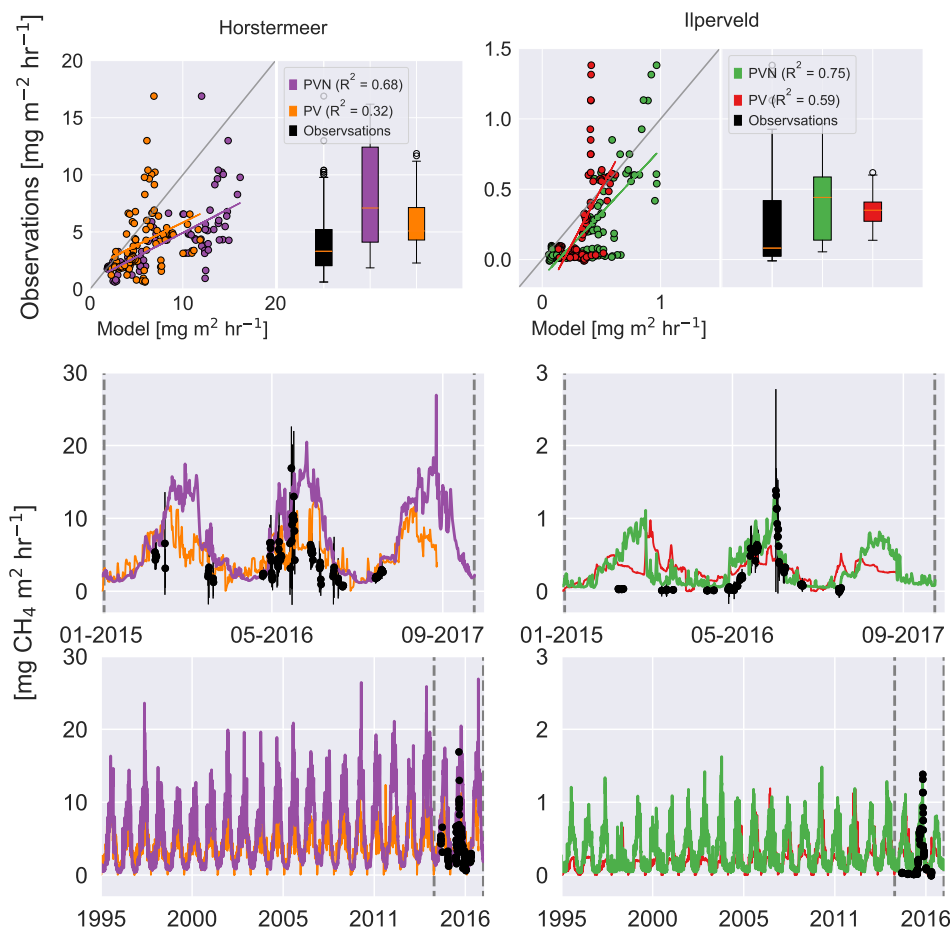
The comparison between the Horstermeer simulation results and observations showed that the model captured the mean daily CO$_2$ fluxes but overestimated CH$_4$ fluxes. The comparison between the Ilperveld simulation results and the observations showed that the model overestimated the mean CO$_2$ fluxes but reproduced the mean and variability of CH$_4$ fluxes.

3.5 Comparison to the PEATLAND-VU model

To understand the impact of including vegetation dynamics, we compare the results of the new PVN model against the results of the pre-existing Peatland-VU model (Fig. 9) and CO$_2$ (Fig. 10). The simulation results are summarised in Table 6. Overall, the PVN model estimated the net annual CH$_4$, CO$_2$, and GHG emissions to be larger than the emissions estimates made by the Peatland-VU model. The Peatland-VU model estimated the annual mean 2015-17 GHG emissions to be 1.3 and 5.9 $\mathrm{kgCO_{2eq}m^{-2}yr^{-1}}$ for the Ilperveld and Horstermeer simulations, respectively, calculated using a 20yr GWP. When calculated using a 100yr GWP, the Peatland-VU model GHG emission estimates for the Horstermeer simulation were 3.8

Figure 9. Simulated and observed methane fluxes at the Horstermeer (left) and Ilperveld (right). The R^2 values are provided for comparison between the new PVN, Peatland-VU model and the observations. In the top panel, the 1:1 line is plotted in grey. The black dots are in situ flux chamber observational measurements in the middle and lower panels. Note the differing x and y axes.

$kgCO_{2eq}m^{-2}yr^{-1}$ (for both periods 2015-17 and 1995-2017). The Peatland-VU GHG emission estimates for the Ilperveld simulation were 1.3 and 1.2 $kgCO_{2eq}m^{-2}yr^{-1}$, for the 2015-17 and 1995-2017 periods, respectively.

The comparison of modelled and measured CH_4 emissions showed that the PVN model performed well, reproducing CH_4 emissions within the spread of observations, in comparison to the Peatland-VU model. The PVN Horstermeer simulation

650 results estimated large mean annual CH_4 emissions (5.1 $kgCO_{2eq}m^{-2}yr^{-1}$) in comparison to the Peatland-VU model (3.2 $kgCO_{2eq}m^{-2}yr^{-1}$) for the period 2015-17. The R^2 value of the PVN model results in comparison to the observations was 0.7 for the Horstermeer simulation and 0.8 for the Ilperveld simulation. In comparison, the Peatland-VU model results produced R^2 values of 0.3 and 0.6 for the Horstermeer and Ilperveld simulations, respectively. The Peatland-VU model showed good skill reproducing the CO_2 fluxes at the Horstermeer site ($R^2 = 0.7$) and less skill at the Ilperveld site ($R^2 = 0.6$). Similarly, the

655 PVN model showed good skill reproducing daily CO_2 fluxes at the Horstermeer site ($R^2 = 0.8$) but less skill at the Ilperveld
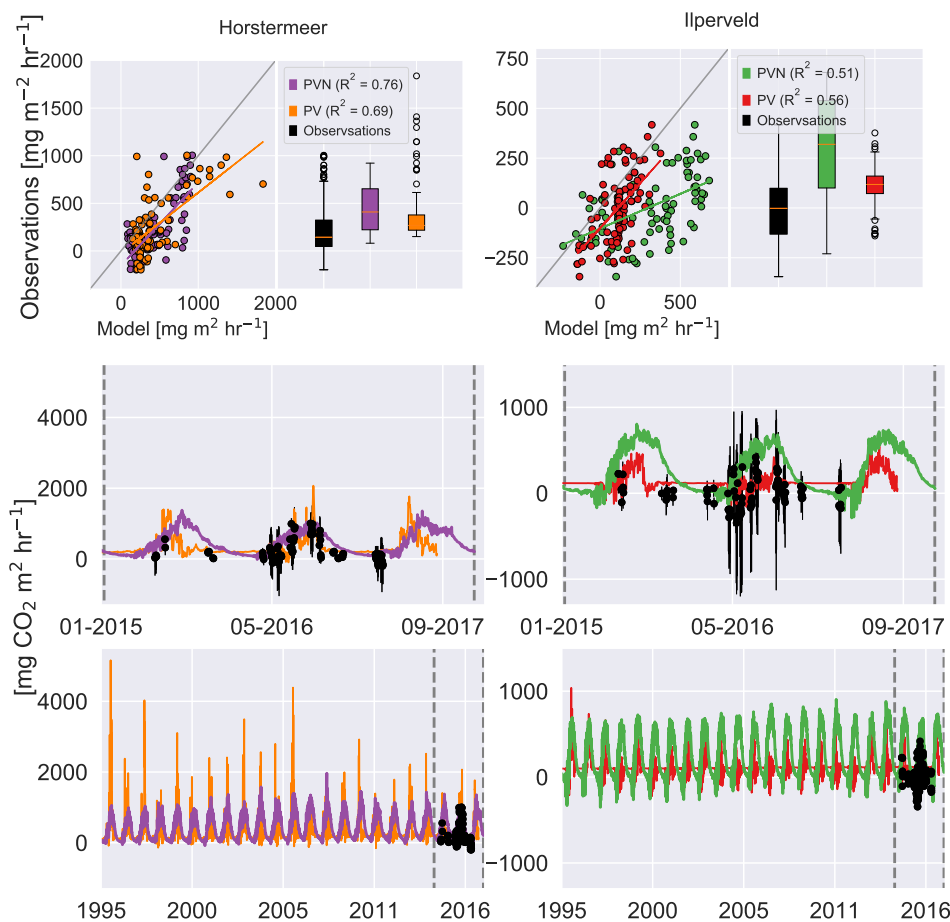
Figure 10. Simulated and observed carbon dioxide fluxes (NEE) at the Horstermeer (left) and Ilperveld (right). The R^2 values are provided for comparison between the new PVN, Peatland-VU model and the observations. In the top panel, the 1:1 line is plotted in grey. The black dots are in situ flux chamber observational measurements in the middle and lower panels. Note the differing x and y axes.

Table 6. Annual average 2015-17 and 1995-2017 CO_2, CH_4, and GHG emissions. All values are expressed as CO_2 equivalents ($kgCO_{2eq}m^{-2}yr^{-1}$) and calculated using 20 (100) year GWP for CH_4 and GHG values.

Site	Model	GHG		CO_2		CH_4	
		2015-17	1995-2017	2015-17	1995-17	2015-17	1995-17
Horstermeer	PVN	8.88 (5.56)	7.96 (5.20)	3.87	3.81	5.01 (1.68)	4.15 (1.40)
Horstermeer	PV	5.90 (3.80)	5.80 (3.81)	2.74	2.81	3.17 (1.07)	2.99 (1.01)
Ilperveld	PVN	2.47 (2.32)	2.41 (2.27)	2.25	2.19	0.22 (0.08)	0.22 (0.08)
Ilperveld	PV	1.27 (1.15)	1.19 (1.08)	1.09	1.03	0.18 (0.06)	0.16 (0.05)

site ($R^2 = 0.6$), as indicated by the linear regression results. Overall, assessment of the linear regression results showed that the behaviour of the PVN model performed well against the observations when compared to the Peatland-VU model.

4 Discussion

We have developed the PVN model, a new dynamic vegetation-peatland-emissions model capable of understanding the role dynamic PFTs have on CO_2 and CH_4 emissions in peatlands. We tested the sensitivity of simulated PFT processes to changing environmental parameters and investigated the impacts of the new schemes introduced into the model that attempt to replicate competition between vegetation types. Here we discuss potential sources of uncertainty, both in the observational data used to evaluate the model results and in the chosen model input parameters. Secondly, we discuss the processes in the model that allow the representation of dynamic vegetation and the ability of these processes to respond to changing environments. Lastly, we discus how the new PVN model compares to its two parent models, the NUCOM-BOG model and the Peatland-VU model, as well as the one other site-specific GHG emissions peatland model that uses dynamic PFTs.

4.1 Sources of uncertainty

4.1.1 Input parameters

It is important to note that the Peatland-VU, NUCOM-BOG and PVN are heavily parameter dependent models. The Peatland-VU model has been shown to reproduce observed fluxes using widely different parameter sets which means that the Peatland-VU model has a strong equifinality of parametrisations (van Huissteden et al., 2009) because there is simply not enough data available to constrain all model dynamics. One aim of introducing PFTs into the Peatland-VU model was to develop a model with greater dependence on observational data (measurable PFT traits) and less dependence on optimised parameters, reducing the equifinality of the model. It is important that improvements of model processes capture the critical processes, but as simply as possible to minimise problems that arise due to the equifinality of parametrisations (Beven and Freer, 2001). The introduction of PFTs allowed several Peatland-VU parameters that were previously calibratable to become observation-informed parameters, whilst introducing few new parameters, thereby the net result is a reduction in the breadth of the parameter space.

4.1.2 Site Heterogeneity and chamber measurements

We compare the findings of this study against other studies that have assessed observed CH_4 fluxes at the Horstermeer site and discuss uncertainties accompanying the chamber measurement technique. The sites simulated in this study pose challenges because they are degraded peatlands where, easily decomposable carbon is likely to have been mineralised (Dorrepaal et al., 2007; Järveoja et al., 2013), peat has been artificially removed for centuries (Erkens et al., 2016), and nutrients added during livestock grazing (Schrier-Uijl et al., 2014). It remains unclear what impacts these events continue to have on present day CO_2 and CH_4 fluxes. Unfortunately, at the time of publication there were no published studies investigating the CO_2 or CH_4 fluxes measured at the Ilperveld site. The CH_4 fluxes observations (0-17 $mgCH_4m^{-2}hr^{-1}$) presented in this study compared well to reported chamber CH_4 fluxes measured at the Horstermeer site from 2003 till 2008 (van Huissteden et al., 2009), in the range of 2-15 $mgCH_4m^{-2}hr^{-1}$, at an area of the site with a varying water table. Interestingly, the CH_4 observations presented mea-

sured in a wet area of the Horstermeer site were more than double the measurements measured in dry areas of the Horstermeer between 2004 and 2006, using the manual chamber technique (Hendriks et al., 2007). The different chamber measurement locations used by the two studies may account for some of the observed differences. Heterogeneous vegetation and heterogeneous water levels relative to the surface are known to impact both automated and manual flux-chamber measurements. For this reason, observational measurements are impacted by the physical placement of flux chambers in the field, leading to potential measurement bias (Speckman et al., 2015; Baldocchi, 2003). At very heterogeneous sites, such as the Horstermeer site, flux strengths vary due to micro-topography (Wania et al., 2010) and chamber measurements have been reported to vary significantly within one site, which may explain differences between studies.

The Horstermeer site has vegetation standing taller than 1m. At times, it was necessary to consider the vegetation height when selecting chamber location to ensure vegetation (even when folded) could fit within measurement chambers. Field measurements that exclude areas covered by tall vegetation may result in a significant underestimation of CO_2 or particularly, CH_4 fluxes. The absence of tall vegetation measurements limits the capacity to test model representations of tall vegetation processes, restricting the ability to predict changes in CO_2 and CH_4 fluxes in the presence of tall vegetation (Pangala et al., 2013). Due to the labor-intensive nature of accumulating chamber observations consistently through time, these observational datasets do not offer complete temporal continuity, creating an intermittency bias. The high cost of AC meant that sites could not be measured simultaneously, leading to an interrupted sampling regime that may bias CO_2 and CH_4 flux estimates (Morin et al., 2014a, 2017). Most chamber measurements were taken during the plant growing season, assuming that the winter fluxes are negligible which has been shown to not always be the case (Morin et al., 2014b). Future studies can benefit from continuous AC measurements.

4.1.3 On the efficacy of simulating dynamic vegetation

The PVN model was developed by building upon the functionality and structure of the Peatland-VU model whilst incorporating vegetation dynamics from the NUCOM model. The model has incorporated vegetation dynamics and enhanced the Peatland-VU model's existing carbon cycling processes. Competition is based on water table depth, temperature, vegetation height and shading. To verify that the model dynamics are robust and to understand the sensitivity of the PFTs, we performed model sensitivity simulations.

Considering that the short grass, *Sphagnum* and brown moss PFTs share similar PFT parameters, these three PFTs can respond somewhat similarly. Whilst the short grass PFT is a non-moss PFT, its parameters are not dissimilar to those of moss PFTs. However, the short grass PFT quickly increases in biomass due to its broad range of temperature and water levels for growth. This means that the short grass PFT provides strong competition against other PFTs. Even though the short grass PFT is height limited, its quickly increasing biomass allows increasing access to PAR, which leads to large amounts of plant respiration, root growth, and net CO_2 fluxes when compared to the *Sphagnum* and brown moss PFTs. With only a shallow root system (maximum 0.1m), moss PFTs have limited abilities to transport below-ground CO_2 and as expected, the total below-ground CO_2 flux is small for mosses. Whilst mosses do not have root structures in reality, we allocated moss PFTs to have a presence in the top 10cm of the soil layer because in the presence of bryophytes, there is often no clear separation

33

between the living moss layer and the soil surface. In this way, we intended to replicate a transition zone. Key differences in the parameters between short grasses and brown mosses are that short grasses are not considered a moss PFT (relevant for height growth and light interception). In the model, moss PFTs have large CH_4 vP values, low leaf maintenance respiration coefficient and biomass senescence values (Table 1). Whilst these differentiations have been somewhat effective, future model versions might consider further ways of distinguishing moss PFTs (especially *Sphagnum*). The presence of *Sphagnum* in SOM increases the acidity of the soil. By influencing the acidity of the soil and limiting the nutrient availability, *Sphagnum* gains an advantage over other plant types because *Sphagnum* flourishes in nutrient-poor conditions (Moore et al., 2007). A useful addition to future model versions may be to adapt the living moss layer to be incorporated into the soil layer, altering the height of the land surface and simulating hummock and hollow microtopography, as well as impacting corresponding soil properties (e.g. pH, DBD).

Largely, decomposition of the peat reservoir led to enhanced CO_2 fluxes, due to a thick aerobic layer, with low water levels. Modeled photosynthesis and plant respiration are dependent on both temperature and water levels. This enables assessment of the impacts of water availability and extreme temperatures on plant type. Future model applications may consider the relationship between water availability and plant dynamics, and particularly the impacts of drought on both plant photosynthetic capacity, respiration, soil respiration, CH_4 production and oxidation.

4.1.4 Impacts of changing temperature input

Studies show that whilst both CH_4 production and oxidation rates are enhanced by warming, the net CH_4 flux increases with warming because CH_4 production increases at a rate faster than oxidation (Granberg et al., 1999). As expected, the PVN model simulated enhanced CH_4 emissions under simulations driven by warmer temperatures and simulated reduced CH_4 emissions under simulations driven by cooler temperatures. *Sphagnum*, tall grasses, and brown mosses showed unexpected results because they released less CH_4 emissions under warmer simulations. This may be indicative of the narrow temperature limits of *Sphagnum* moss (Gunnarsson et al., 2004). The impacts of temperature on model processes are three-fold. Firstly, the amount of photosynthesis, and plant respiration performed is dependent on the ideal and tolerated PFT growth temperatures. Secondly, the amount of litter converted to below-ground SOM reservoirs is dependent on soil temperatures, where warmer soil temperatures lead to larger amount of litter converted to below-ground reservoirs. Thirdly, decomposition of below-ground SOM is dependent on soil layer temperature (as well as pH, saturation etc.), where soil layers closer to the surface are warmer. Thereby, temperature influences the PFT abundance, size of litter and below-ground SOM reservoirs available for decomposition, and the efficiency of below-ground SOM decomposition in the model. The results of our sensitivity analyses are in agreement with field studies which have found CH_4 emissions are typically higher when dominated by *Carex*, than *Eriophorum* or *Juncus* (Ström et al., 2005; Jackowicz-Korczyński et al., 2010). This is likely partly due to the presence of aerenchyma and partly due to differing litter quality and rates of carbon turnover (Christensen et al., 2003; Ström et al., 2015).

4.1.5 Belowground decomposition

Enabling different PFTs to contribute to, oxidise, and decompose different below-ground SOM pools, impacted simulated CO_2 and CH_4 fluxes. Decomposition in the PVN model is dependent on the decomposition rates of different PFTs. Decomposition rates have been found to differ between forbs, graminoids, deciduous shrubs, and evergreen shrubs (Dorrepaal et al., 2006, 2007, 2009). The peat SOM pool of moss PFTs contribute to CO_2 and CH_4 fluxes because (*Sphagnum*) mosses are the primary peat-contributing plant and mosses (especially *Sphagnum*) have slow decomposition rates (Hobbie et al., 2000). Moss PFTs are the only PFTs able to contribute to the peat SOM pool which means that the CH_4 fluxes arising from decomposition of the peat SOM pool are only transferred to the surface by moss PFTs. Future modelling efforts could work to improve the representation of peat decomposition, whereby CO_2 fluxes resulting from the decomposition of peat can be transferred to the surface by both moss and non-moss PFTs. Mosses are prescribed to have maximum 0.1m roots when the model is initialised and remain constant throughout the model simulation. Mosses do not have an above-ground litter layer and instead their living biomass after senescence, is added directly to the below-ground SOM.

4.1.6 Root distribution representation

Plant transported CH_4 and aerobic CO_2 production process are dependent on root mass and independent of above-ground biomass. In the model, the below-ground CO_2 flux is comprised of CO_2 produced by peat, root exudates, litter, roots, microbial biomass, humic matter, and CH_4 oxidation. Root traits play an important role in species competition and processes such as leaf:root allocation, turnover, root stocks, and root distributions have been shown to be dependent on climate, species, and land cover type (Smithwick et al., 2014), particularly in Arctic and boreal systems (Iversen et al., 2015). Root exudation plays an important role in the supply of substrates that can later be metabolised into CH_4 (Aulakh et al., 2001; Waldo et al., 2019), where the fraction of below-ground production that consists of exudates (REX) was an important parameter impacting CH_4 production in the model. Next to this, the parameter representing root aerenchyma (PlOx) played a role in the oxidation of CH_4 (Walter and Heimann, 2000). These processes as well as plant transported CH_4 are only possible from soil layers with roots present (Bansal et al., 2020; Walter and Heimann, 2000). For this reason, the parameter representing maximum root depth (MRD) played a role in the production, oxidation, and transport of CH_4, where the relative impact of each of these processes on surface CH_4 fluxes are dependent on PFT properties.

Root distribution structural representation is important to reliably simulate CO_2 and CH_4 fluxes in the model. Land surface models have, for the most part, used exponential relationships to describe root distribution (Smithwick et al., 2014; Zeng, 2001). Advances have been made developing knowledge and observational data of root distributions in boreal peatland systems. Whilst the exponential relationship is representative for several peatland plant types, an alternative root representation to the exponential relationship may be relevant for certain peatland plant types (Clemmensen et al., 2013; Iversen et al., 2015). Future model versions may consider introducing alternative root representations.

4.1.7 The impact of harvests on plant competition

The inclusion of harvest has proven necessary to reproduce the seasonal variability of emissions in grasslands and croplands, where crop harvests occur (Van den Hoof et al., 2011). Whilst CO_2 emissions were reduced with increased harvest frequency, these emissions are not considering off-site decomposition of harvested biomass. The harvest method implemented in the PVN model was similar to the instantaneous harvest method featured in other dynamic vegetation models (such as JULES, Littleton et al. (2020)), where the plant is reduced to a certain set height and living biomass and LAI are subsequently adjusted accordingly. JULES assumes 100% of lost biomass is harvested whilst killing off a proportion of below- ground biomass that is converted to litter. The PVN model assumes 20% of harvested biomass is lost to litter and does not account for root death. The increased litter layer leads to enhanced emissions resulting from the decomposition of the litter layer. The PFT living biomass is reduced by the proportional biomass lost, assuming the plant's biomass is uniformly distributed with height, and LAI is recalculated. Root mass observational measurements over time as well as observational data on the impact of harvests on plant productivity would further improve model representations of harvests. Further assessment may investigate in what ways the photosynthesising, and gas conduit capacities of plants are further reduced in the days after harvest and how this can be better captured by the model.

4.2 Comparison to other site-specific peatland GHG emission models

Here we compare the functionality of the new PVN model against its parent models; the Peatland-VU and NUCOM-BOG models. We then also compare the functionality of the PVN model against the functionality of PEATBOG, the one other site-specific peatland GHG emissions model that includes dynamic vegetation (Table S1). We have developed a new model capable of understanding the role dynamic PFTs have on CO_2 and CH_4 emissions in peatlands. The PVN model simulation results estimated the 1995-2017 annually averaged net GHG budget to be larger than the Peatland-VU model, at both sites. We suspect that there are two reasons for this. The first being a trade-off between enhanced CO_2 emissions or enhanced CH_4 emissions. In both the Peatland-VU and PVN models, the CO_2 processes are calculated first. Calibration of the photosynthesis and plant respiration related parameters impacts the amount of CO_2 available for CH_4 production. Photosynthesis and leaf respiration mechanisms were the greatest cause of uncertainty in the model's ability to reproduce the net GHG budget. Future model versions, may consider ways to constrain the net CO_2 flux by improving the response of photosynthesis to environmental variables. To improve upon this in future model versions it may be useful to consider the representation of below-ground carbon decomposition. The below-ground CH_4 pool in the Peatland-VU model increased consistently during the model simulation and therefore, an increasing quantity of CH_4 was released from the soil profile throughout the simulation, indicating that the fluxes were likely underestimated early in the simulation. The PVN model prescribes each PFT to have root and shoot mass and root depths. This enables each PFT to access different soil layers, and below-ground CH_4 and carbon pools, potentially impacting the longterm variability of CH_4 emissions. When compared to observed fluxes, the results indicated that the CO_2 scheme in the PVN model may have limited skill when applied to peatland sites of certain physical properties. These results cannot be

compared with previous modelling studies because the Peatland-VU CO_2 production scheme results have not been published since the CO_2 production scheme was introduced by Mi et al. (2014) for assessment of the impact on simulated CH_4 fluxes.

The NUCOM model was developed to assess the impact of climate change on bog ecosystems by analysing simulations lasting 200-500 years. Running the model over time periods similar to the NUCOM's 1760–2000 simulation period, can be used to assess the model's ability to reproduce shifts in vegetation in response to climate variability. This would require model evaluation using multi-centennial observational data, such as macrofossil evidence. To further investigate the impact of climate change on peatland ecosystems future studies may consider using macrofossil data in combination with forward or backward multi-decadal or multi-centennial climate projections.

The PEATBOG model (Wu and Blodau, 2013) is the one other site-specific peatland model that simulates CO_2 and CH_4 fluxes and includes competition between moss, shrub, and graminoid PFTs. The PEATBOG model has simulated the Mer Bleue Bog in Canada, a pristine (untouched) raised acidic ombrotrophic bog, over a 6 year period. The Mer Bleue Bog is a nutrient-poor bog, unlike the two sites assessed in this study. The net annual GHG emissions for the Mer Bleue Bog site were small, approximately 0.02% of the GHG emissions observed at the Ilperveld field site in the Netherlands. Peat has been accumulating at this site since 8400 calyrBP and has developed a peat depth of 6m in the center. The PEATBOG model is a complex model that simulates many of the same processes as the PVN model but beyond this also includes representation of the nitrogen cycling, electron accepting processes, dissolved inorganic and organic carbon, and subsequent CO_2 and CH_4 run-off. The PEATBOG model underestimated the annual net GHG emissions (net ecosystem carbon balance), by approximately half of observed field observations. Wu and Blodau (2013) noted the sensitivity of the PEATBOG model to temperature, reporting that $1°C$ of temperature change was enough to initiate a model bias, swaying the model from a source to a sink. This is concurrent with the results of the sensitivity testing performed in this study, which showed that changes in air temperature had large impacts on both CO_2 and CH_4 emissions. Plot-scale model inter-comparison efforts could help improve the representation of small-scale processes in peatland models. However, the breadth of observational data required to run and test site-specific models, make site specific model inter-comparison efforts cumbersome and difficult.

5 Conclusions

Here, we present Peatland-VU-NUCOM v1.0 (PVN), a new site-specific peatland dynamic vegetation emissions model. By including plant-environmental feedbacks, the model can serve wetland management by estimating changes in the GHG balance of peatland sites in response to environmental change, such as changing air temperatures, water level or precipitation/evapotranspiration; or new management decisions, such as raising the water table, vegetation restoration or modifying mowing regimes. The PVN model was designed to simulate plant competition above and below-ground, whilst developing carbon pools for the production and oxidation of CH_4 and CO_2. PFTs compete for light where where production and respiration are dependent on ideal temperature and water levels. Structural differences in vegetation root, exudation, and stem representation impact CH_4 production, oxidation, and transport. Peatlands are one of the most important carbon storing ecosystems. The challenges facing our understanding of the carbon balance and CH_4 dynamics subsequent to the rewetting of previously

850 managed peatlands are numerous. One challenge is the ability of site-specific peatland models to reproduce CH_4 fluxes, particularly in relation to plant functioning. This question is particularly timely because there exists an urgent need to restore drained peatlands to reduce land subsidence whilst limiting GHG emissions. We show that the PVN model is able to reproduce plant biomass fractions, CH_4 and CO_2 fluxes under changing environmental conditions. This confirms that the model provides the capability to understand the relationship between peatland plant dynamics, CH_4 and CO_2 emissions. The PVN model is a

855 relevant tool that can be used to optimize vegetation management with the goal to reduce GHG emissions.

References

Alhoz, K., Kenesei, K., Papageorgiou, M., Keurentjes, E. E. M., and de Jong, M.: Improved AHN3 Gridded DTM/DSM, 2020.

Aulakh, M. S., Wassmann, R., Bueno, C., and Rennenberg, H.: Impact of root exudates of different cultivars and plant development stages of rice (Oryza sativa L.) on methane production in a paddy soil, Plant and Soil, 230, 77–86, https://doi.org/10.1023/A:1004817212321, 2001.

Baldocchi, D. D.: Assessing the eddy covariance technique for evaluating carbon dioxide exchange rates of ecosystems: Past, present and future, Global Change Biology, 9, 479–492, https://doi.org/10.1046/j.1365-2486.2003.00629.x, 2003.

Baldocchi, D. D. and Harley, P. C.: Scaling carbon dioxide and water vapour exchange from leaf to canopy in a deciduous forest. II. Model testing and application, Plant, Cell and Environment, 18, 1157–1173, https://doi.org/10.1111/j.1365-3040.1995.tb00626.x, 1995.

Ballantyne, D. M., Hribljan, J. A., Pypker, T. G., and Chimner, R. A.: Long-term water table manipulations alter peatland gaseous carbon fluxes in Northern Michigan, Wetlands Ecology and Management, 22, 35–47, https://doi.org/10.1007/s11273-013-9320-8, 2014.

Bansal, S., Johnson, O. F., Meier, J., and Zhu, X.: Vegetation Affects Timing and Location of Wetland Methane Emissions, Journal of Geophysical Research: Biogeosciences, 125, https://doi.org/10.1029/2020JG005777, 2020.

Bao, T., Jia, G., and Xu, X.: Weakening greenhouse gas sink of pristine wetlands under warming, Nature Climate Change, 13, https://doi.org/10.1038/s41558-023-01637-0, 2023.

Basile-Doelsch, I., Balesdent, J., and Pellerin, S.: Reviews and syntheses: The mechanisms underlying carbon storage in soil, Biogeosciences, 17, 5223–5242, https://doi.org/10.5194/bg-17-5223-2020, 2020.

Beven, K. and Freer, J.: Equifinality, data assimilation, and uncertainty estimation in mechanistic modelling of complex environmental systems using the GLUE methodology, Journal of Hydrology, 249, 11–29, https://doi.org/10.1016/S0022-1694(01)00421-8, 2001.

Boonman, J., Hefting, M. M., Van Huissteden, C. J., Van Den Berg, M., Van Huissteden, J., Erkens, G., Melman, R., and Van Der Velde, Y.: Cutting peatland CO2 emissions with water management practices, Biogeosciences, 19, 5707–5727, https://doi.org/10.5194/bg-19-5707-2022, https://doi.org/10.5194/bg-19-5707-2022, 2022.

Box, J. E., Colgan, W. T., Christensen, T. R., Schmidt, N. M., Lund, M., Parmentier, F. J. W., Brown, R., Bhatt, U. S., Euskirchen, E. S., Romanovsky, V. E., Walsh, J. E., Overland, J. E., Wang, M., Corell, R. W., Meier, W. N., Wouters, B., Mernild, S., Mård, J., Pawlak, J., and Olsen, M. S.: Key indicators of Arctic climate change: 1971-2017, Environmental Research Letters, 14, https://doi.org/10.1088/1748-9326/aafc1b, 2019.

Bridgham, S. D., Cadillo-Quiroz, H., Keller, J. K., and Zhuang, Q.: Methane emissions from wetlands: Biogeochemical, microbial, and modeling perspectives from local to global scales, Global Change Biology, 19, 1325–1346, https://doi.org/10.1111/gcb.12131, 2013.

Bubier, J.: The Relationship of Vegetation to Methane Emission and Hydrochemical Gradients in Northern Peatlands, Journal of Ecology, 83, 403–420, http://www.jstor.org/stable/2261594, 2016.

Chaney, N. W., Sheffield, J., Villarini, G., and Wood, E. F.: Development of a high-resolution gridded daily meteorological dataset over sub-Saharan Africa: Spatial analysis of trends in climate extremes, Journal of Climate, 27, 5815–5835, https://doi.org/10.1175/JCLI-D-13-00423.1, 2014.

Christensen, T. R., Ekberg, A., Ström, L., Mastepanov, M., Panikov, N., Öquist, M., Svensson, B. H., Nykänen, H., Martikainen, P. J., and Oskarsson, H.: Factors controlling large scale variations in methane emissions from wetlands, Geophysical Research Letters, 30, 1–4, https://doi.org/10.1029/2002GL016848, 2003.

Churkina, G., Running, S. W., and Schloss, A. L.: Comparing global models of terrestrial net primary productivity (NPP): The importance of water availability, Global Change Biology, 5, 46–55, https://doi.org/10.1046/j.1365-2486.1999.00006.x, 1999.

910 Clemmensen, K. E., Bahr, A., Ovaskainen, O., Dahlberg, A., Ekblad, A., Wallander, H., Stenlid, J., Finlay, R. D., Wardle, D. A., and Lindahl, B. D.: Roots and Associated Fungi Drive Long-Term Carbon Sequestration in Boreal Forest, Science, 339, 1615–1618, https://doi.org/10.1126/science.1231923, https://www.sciencemag.org/lookup/doi/10.1126/science.1231923, 2013.

Crow, S. E. and Wieder, R. K.: Sources of CO_2 emission from a northern peatland: Root respiration, exudation, and decomposition, Ecology, 86, 1825–1834, https://doi.org/10.1890/04-1575, 2005.

915 Davidson, E. and Janssens, I. A.: Temperature sensitivity of soil carbon decomposition and feedbacks to climate change., Nature, 440, 165–173, https://doi.org/10.1038/nature04514, 2006.

De Boeck, H. J., Dreesen, F. E., Janssens, I. A., and Nijs, I.: Whole-system responses of experimental plant communities to climate extremes imposed in different seasons, New Phytologist, 189, 806–817, https://doi.org/10.1111/j.1469-8137.2010.03515.x, http://www.ncbi.nlm.nih.gov/pubmed/21054412, 2011.

920 De La Motte, L. G., Beauclaire, Q., Heinesch, B., Cuntz, M., Foltýnová, L., Šigut, L., Kowalska, N., Manca, G., Ballarin, I. G., Vincke, C., Roland, M., Ibrom, A., Lousteau, D., Siebicke, L., Neiryink, J., and Longdoz, B.: Non-stomatal processes reduce gross primary productivity in temperate forest ecosystems during severe edaphic drought: Edaphic drought in forest ecosystems, Philosophical Transactions of the Royal Society B: Biological Sciences, 375, https://doi.org/10.1098/rstb.2019.0527, 2020.

De Lange, W. J., Prinsen, G. F., Hoogewoud, J. C., Veldhuizen, A. A., Verkaik, J., Oude Essink, G. H., Van Walsum, P. E., Delsman, 925 J. R., Hunink, J. C., Massop, H. T. L., and Kroon, T.: An operational, multi-scale, multi-model system for consensus-based, integrated water management and policy analysis: The Netherlands Hydrological Instrument., Environmental Modelling and Software, 59, 98–108, https://doi.org/10.1016/j.envsoft.2014.05.009, http://dx.doi.org/10.1016/j.envsoft.2014.05.009, 2014.

Dick, J. J., Tetzlaff, D., Birkel, C., and Soulsby, C.: Modelling landscape controls on dissolved organic carbon sources and fluxes to streams, Biogeochemistry, 122, 361–374, https://doi.org/10.1007/s10533-014-0046-3, http://link.springer.com/10.1007/s10533-014-0046-3, 2015.

930 Dorrepaal, E., Aerts, R., Cornelissen, J. H., Van Logtestijn, R. S., and Callaghan, T. V.: Sphagnum modifies climate-change impacts on subarctic vascular bog plants, Functional Ecology, 20, 31–41, https://doi.org/10.1111/j.1365-2435.2006.01076.x, 2006.

Dorrepaal, E., Cornelissen, J. H., and Aerts, R.: Changing leaf litter feedbacks on plant production across contrasting sub-arctic peatland species and growth forms, Oecologia, 151, 251–261, https://doi.org/10.1007/s00442-006-0580-3, 2007.

Dorrepaal, E., Toet, S., Van Logtestijn, R. S., Swart, E., Van De Weg, M. J., Callaghan, T. V., and Aerts, R.: Carbon respiration from 935 subsurface peat accelerated by climate warming in the subarctic, Nature, 460, 616–619, https://doi.org/10.1038/nature08216, http://dx.doi.org/10.1038/nature08216, 2009.

Erkens, G., Van Der Meulen, M. J., and Middelkoop, H.: Double trouble: Subsidence and CO_2 respiration due to 1,000 years of Dutch coastal peatlands cultivation, Hydrogeology Journal, 24, 551–568, https://doi.org/10.1007/s10040-016-1380-4, 2016.

Evans, C. D., Peacock, M., Baird, A. J., Artz, R. R., Burden, A., Callaghan, N., Chapman, P. J., Cooper, H. M., Coyle, M., Craig, E., Cumming, 940 A., Dixon, S., Gauci, V., Grayson, R. P., Helfter, C., Heppell, C. M., Holden, J., Jones, D. L., Kaduk, J., Levy, P., Matthews, R., McNamara, N. P., Misselbrook, T., Oakley, S., Page, S. E., Rayment, M., Ridley, L. M., Stanley, K. M., Williamson, J. L., Worrall, F., and Morrison, R.: Overriding water table control on managed peatland greenhouse gas emissions, Nature, 593, 548–552, https://doi.org/10.1038/s41586-021-03523-1, http://dx.doi.org/10.1038/s41586-021-03523-1, 2021.

Frolking, S. and Roulet, N. T.: Holocene radiative forcing impact of northern peatland carbon accumulation and methane emissions, Global 945 Change Biology, 13, 1079–1088, https://doi.org/10.1111/j.1365-2486.2007.01339.x, 2007.

Gerten, D., Schaphoff, S., Haberlandt, U., Lucht, W., and Sitch, S.: Terrestrial vegetation and water balance - Hydrological evaluation of a dynamic global vegetation model, Journal of Hydrology, 286, 249–270, https://doi.org/10.1016/j.jhydrol.2003.09.029, 2004.

Geurts, J. and Fritz, C.: Paludiculture pilots and experiments with focus on cattail and reed in the Netherlands. Technical, Tech. rep., Radboud University Nijmegen, Nijmegen, https://repository.ubn.ru.nl/handle/2066/192628, 2018.

950   Gorham, E.: Shoot height, weight and standing crop in relation to density of monospecific plant stands, Nature, 279, 148–150, https://doi.org/10.1038/279148a0, https://www.nature.com/articles/279148a0, 1979.

Graf, M. and Rochefort, L.: Examining the peat-accumulating potential of fen vegetation in the context of fen restoration of harvested peatlands, Ecoscience, 16, 158–166, https://doi.org/10.2980/16-2-3128, 2009.

Granberg, G., Grip, H., Ottosson Löfvenius, M., Sundh, I., Svensson, B. H., and Nilsson, M.: A simple model for simula-
955   tion of water content, soil frost, and soil temperatures in boreal mixed mires, Water Resources Research, 35, 3771–3782, https://doi.org/10.1029/1999WR900216, 1999.

Gunnarsson, U., Granberg, G., and Nilsson, M.: Growth, production and interspecific competition in Sphagnum: Effects of temperature, nitrogen and sulphur treatments on a boreal mire, New Phytologist, 163, 349–359, https://doi.org/10.1111/j.1469-8137.2004.01108.x, 2004.

960   Günther, A., Barthelmes, A., Huth, V., Joosten, H., Jurasinski, G., Koebsch, F., and Couwenberg, J.: Prompt rewetting of drained peatlands reduces climate warming despite methane emissions, Nature Communications, 11, 1644, https://doi.org/10.1038/s41467-020-15499-z, http://www.nature.com/articles/s41467-020-15499-z, 2020.

Gupta, H. V., Kling, H., Yilmaz, K. K., and Martinez, G. F.: Decomposition of the mean squared error and NSE performance criteria: Implications for improving hydrological modelling, Journal of Hydrology, 377, 80–91, https://doi.org/10.1016/j.jhydrol.2009.08.003, http:
965   //dx.doi.org/10.1016/j.jhydrol.2009.08.003, 2009.

Harpenslager, S. F., van den Elzen, E., Kox, M. A., Smolders, A. J., Ettwig, K. F., and Lamers, L. P.: Rewetting former agricultural peatlands: Topsoil removal as a prerequisite to avoid strong nutrient and greenhouse gas emissions, Ecological Engineering, 84, 159–168, https://doi.org/10.1016/j.ecoleng.2015.08.002, http://dx.doi.org/10.1016/j.ecoleng.2015.08.002, 2015.

Haxeltine, A. and Prentice, I. C.: BIOME3: An equilibrium terrestrial biosphere model based on ecophysiological constraints, resource avail-
970   ability, and competition among plant functional types, Global Biogeochemical Cycles, 10, 693–709, https://doi.org/10.1029/96GB02344, http://doi.wiley.com/10.1029/96GB02344, 1996.

Heijmans, M. and Berendse, F.: NUCOM: a dynamic vegetation model for peatlands and tundra including nitrogen cycling and mosses, 2008.

Heijmans, M. M., Mauquoy, D., Van Geel, B., and Berendse, F.: Long-term effects of climate change on vegetation and carbon dynamics
975   in peat bogs, Journal of Vegetation Science, 19, 307–320, https://doi.org/10.3170/2008-8-18368, https://www.scopus.com/inward/record.url?eid=2-s2.0-41849115693&partnerID=40&md5=650f510b7f8fb783728dc3e00073b873, 2008.

Hendriks, D. M., Van Huissteden, J., Dolman, A. J., and Van Der Molen, M. K.: The full greenhouse gas balance of an abandoned peat meadow, Biogeosciences, 4, 411–424, https://doi.org/10.5194/bg-4-411-2007, 2007.

Hobbie, S. E., Schimel, J. P., Trumbore, S. E., and Randerson, J. R.: Controls over carbon storage and turnover in high-latitude soils, Global
980   Change Biology, 6, 196–210, https://doi.org/10.1046/j.1365-2486.2000.06021.x, 2000.

Högberg, P., Nordgren, A., Buchmann, N., Taylor, A. F., Ekblad, A., Högberg, M. N., Nyberg, G., Ottosson-Löfvenius, M., and Read, D. J.: Large-scale forest girdling shows that current photosynthesis drives soil respiration, Nature, 411, 789–792, https://doi.org/10.1038/35081058, 2001.

Huang, S., Titus, S. J., and Wiens, D. P.: Comparison of nonlinear height-diameter functions for major Alberta tree species, Canadian Journal of Forest Research, 22, 1297–1304, https://doi.org/10.1139/x92-172, https://cdnsciencepub.com/doi/10.1139/x92-172http://www.nrcresearchpress.com/doi/10.1139/x92-172, 1992.

Iversen, C. M., Sloan, V. L., Sullivan, P. F., Euskirchen, E. S., Mcguire, A. D., Norby, R. J., Walker, A. P., Warren, J. M., and Wullschleger, S. D.: The unseen iceberg: Plant roots in arctic tundra, New Phytologist, 205, 34–58, https://doi.org/10.1111/nph.13003, http://www.ncbi.nlm.nih.gov/pubmed/25209220https://onlinelibrary.wiley.com/doi/10.1111/nph.13003, 2015.

Jaatinen, K., Laiho, R., Vuorenmaa, A., Del Castillo, U., Minkkinen, K., Pennanen, T., Penttilä, T., and Fritze, H.: Responses of aerobic microbial communities and soil respiration to water-level drawdown in a northern boreal fen, Environmental Microbiology, 10, 339–353, https://doi.org/10.1111/j.1462-2920.2007.01455.x, 2008.

Jackowicz-Korczyński, M., Christensen, T. R., Bäckstrand, K., Crill, P., Friborg, T., Mastepanov, M., and Ström, L.: Annual cycle of methane emission from a subarctic peatland, Journal of Geophysical Research: Biogeosciences, 115, 1–10, https://doi.org/10.1029/2008JG000913, 2010.

Jackson, R. B., Canadell, J., Ehleringer, J. R., Mooney, H. A., Sala, O. E., and Schulze, E. D.: A global analysis of root distributions for terrestrial biomes, Oecologia, 108, 389–411, https://doi.org/10.1007/BF00333714, 1996.

Järveoja, J., Laht, J., Maddison, M., Soosaar, K., Ostonen, I., and Mander, Ü.: Mitigation of greenhouse gas emissions from an abandoned Baltic peat extraction area by growing reed canary grass: Life-cycle assessment, Regional Environmental Change, 13, 781–795, https://doi.org/10.1007/s10113-012-0355-9, 2013.

Kattge, J., Díaz, S., Lavorel, S., Prentice, I. C., Leadley, P., Bönisch, G., Garnier, E., Westoby, M., Reich, P. B., Wright, I. J., Cornelissen, J. H., Violle, C., Harrison, S. P., Van Bodegom, P. M., Reichstein, M., Enquist, B. J., Soudzilovskaia, N. A., Ackerly, D. D., Anand, M., Atkin, O., Bahn, M., Baker, T. R., Baldocchi, D., Bekker, R., Blanco, C. C., Blonder, B., Bond, W. J., Bradstock, R., Bunker, D. E., Casanoves, F., Cavender-Bares, J., Chambers, J. Q., Chapin, F. S., Chave, J., Coomes, D., Cornwell, W. K., Craine, J. M., Dobrin, B. H., Duarte, L., Durka, W., Elser, J., Esser, G., Estiarte, M., Fagan, W. F., Fang, J., Fernández-Méndez, F., Fidelis, A., Finegan, B., Flores, O., Ford, H., Frank, D., Freschet, G. T., Fyllas, N. M., Gallagher, R. V., Green, W. A., Gutierrez, A. G., Hickler, T., Higgins, S. I., Hodgson, J. G., Jalili, A., Jansen, S., Joly, C. A., Kerkhoff, A. J., Kirkup, D., Kitajima, K., Kleyer, M., Klotz, S., Knops, J. M., Kramer, K., Kühn, I., Kurokawa, H., Laughlin, D., Lee, T. D., Leishman, M., Lens, F., Lenz, T., Lewis, S. L., Lloyd, J., Llusià, J., Louault, F., Ma, S., Mahecha, M. D., Manning, P., Massad, T., Medlyn, B. E., Messier, J., Moles, A. T., Müller, S. C., Nadrowski, K., Naeem, S., Niinemets, Ü., Nöllert, S., Nüske, A., Ogaya, R., Oleksyn, J., Onipchenko, V. G., Onoda, Y., Ordoñez, J., Overbeck, G., Ozinga, W. A., Patiño, S., Paula, S., Pausas, J. G., Peñuelas, J., Phillips, O. L., Pillar, V., Poorter, H., Poorter, L., Poschlod, P., Prinzing, A., Proulx, R., Rammig, A., Reinsch, S., Reu, B., Sack, L., Salgado-Negret, B., Sardans, J., Shiodera, S., Shipley, B., Siefert, A., Sosinski, E., Soussana, J. F., Swaine, E., Swenson, N., Thompson, K., Thornton, P., Waldram, M., Weiher, E., White, M., White, S., Wright, S. J., Yguel, B., Zaehle, S., Zanne, A. E., and Wirth, C.: TRY - a global database of plant traits, Global Change Biology, 17, 2905–2935, https://doi.org/10.1111/j.1365-2486.2011.02451.x, 2011.

Kattge, J., Bönisch, G., Díaz, S., Lavorel, S., Prentice, I. C., Leadley, P., Tautenhahn, S., Werner, G. D., Aakala, T., Abedi, M., Acosta, A. T., Adamidis, G. C., Adamson, K., Aiba, M., Albert, C. H., Alcántara, J. M., Alcázar C, C., Aleixo, I., Ali, H., Amiaud, B., Ammer, C., Amoroso, M. M., Anand, M., Anderson, C., Anten, N., Antos, J., Apgaua, D. M. G., Ashman, T. L., Asmara, D. H., Asner, G. P., Aspinwall, M., Atkin, O., Aubin, I., Baastrup-Spohr, L., Bahalkeh, K., Bahn, M., Baker, T., Baker, W. J., Bakker, J. P., Baldocchi, D., Baltzer, J., Banerjee, A., Baranger, A., Barlow, J., Barneche, D. R., Baruch, Z., Bastianelli, D., Battles, J., Bauerle, W., Bauters, M., Bazzato, E., Beckmann, M., Beeckman, H., Beierkuhnlein, C., Bekker, R., Belfry, G., Belluau, M., Beloiu, M., Benavides, R., Benomar,

L., Berdugo-Lattke, M. L., Berenguer, E., Bergamin, R., Bergmann, J., Bergmann Carlucci, M., Berner, L., Bernhardt-Römermann, M., Bigler, C., Bjorkman, A. D., Blackman, C., Blanco, C., Blonder, B., Blumenthal, D., Bocanegra-González, K. T., Boeckx, P., Bohlman, S., Böhning-Gaese, K., Boisvert-Marsh, L., Bond, W., Bond-Lamberty, B., Boom, A., Boonman, C. C., Bordin, K., Boughton, E. H., Boukili, V., Bowman, D. M., Bravo, S., Brendel, M. R., Broadley, M. R., Brown, K. A., Bruelheide, H., Brumnich, F., Bruun, H. H., Bruy, D., Buchanan, S. W., Bucher, S. F., Buchmann, N., Buitenwerf, R., Bunker, D. E., Bürger, J., Burrascano, S., Burslem, D. F., Butterfield, B. J., Byun, C., Marques, M., Scalon, M. C., Caccianiga, M., Cadotte, M., Cailleret, M., Camac, J., Camarero, J. J., Campany, C., Campetella, G., Campos, J. A., Cano-Arboleda, L., Canullo, R., Carbognani, M., Carvalho, F., Casanoves, F., Castagneyrol, B., Catford, J. A., Cavender-Bares, J., Cerabolini, B. E., Cervellini, M., Chacón-Madrigal, E., Chapin, K., Chapin, F. S., Chelli, S., Chen, S. C., Chen, A., Cherubini, P., Chianucci, F., Choat, B., Chung, K. S., Chytrý, M., Ciccarelli, D., Coll, L., Collins, C. G., Conti, L., Coomes, D., Cornelissen, J. H., Cornwell, W. K., Corona, P., Coyea, M., Craine, J., Craven, D., Cromsigt, J. P., Csecserits, A., Cufar, K., Cuntz, M., da Silva, A. C., Dahlin, K. M., Dainese, M., Dalke, I., Dalle Fratte, M., Dang-Le, A. T., Danihelka, J., Dannoura, M., Dawson, S., de Beer, A. J., De Frutos, A., De Long, J. R., Dechant, B., Delagrange, S., Delpierre, N., Derroire, G., Dias, A. S., Diaz-Toribio, M. H., Dimitrakopoulos, P. G., Dobrowolski, M., Doktor, D., Dřevojan, P., Dong, N., Dransfield, J., Dressler, S., Duarte, L., Ducouret, E., Dullinger, S., Durka, W., Duursma, R., Dymova, O., E-Vojtkó, A., Eckstein, R. L., Ejtehadi, H., Elser, J., Emilio, T., Engemann, K., Erfanian, M. B., Erfmeier, A., Esquivel-Muelbert, A., Esser, G., Estiarte, M., Domingues, T. F., Fagan, W. F., Fagúndez, J., Falster, D. S., Fan, Y., Fang, J., Farris, E., Fazlioglu, F., Feng, Y., Fernandez-Mendez, F., Ferrara, C., Ferreira, J., Fidelis, A., Finegan, B., Firn, J., Flowers, T. J., Flynn, D. F., Fontana, V., Forey, E., Forgiarini, C., François, L., Frangipani, M., Frank, D., Frenette-Dussault, C., Freschet, G. T., Fry, E. L., Fyllas, N. M., Mazzochini, G. G., Gachet, S., Gallagher, R., Ganade, G., Ganga, F., García-Palacios, P., Gargaglione, V., Garnier, E., Garrido, J. L., de Gasper, A. L., Gea-Izquierdo, G., Gibson, D., Gillison, A. N., Giroldo, A., Glasenhardt, M. C., Gleason, S., Gliesch, M., Goldberg, E., Göldel, B., Gonzalez-Akre, E., Gonzalez-Andujar, J. L., González-Melo, A., González-Robles, A., Graae, B. J., Granda, E., Graves, S., Green, W. A., Gregor, T., Gross, N., Guerin, G. R., Günther, A., Gutiérrez, A. G., Haddock, L., Haines, A., Hall, J., Hambuckers, A., Han, W., Harrison, S. P., Hattingh, W., Hawes, J. E., He, T., He, P., Heberling, J. M., Helm, A., Hempel, S., Hentschel, J., Hérault, B., Hereş, A. M., Herz, K., Heuertz, M., Hickler, T., Hietz, P., Higuchi, P., Hipp, A. L., Hirons, A., Hock, M., Hogan, J. A., Holl, K., Honnay, O., Hornstein, D., Hou, E., Hough-Snee, N., Hovstad, K. A., Ichie, T., Igić, B., Illa, E., Isaac, M., Ishihara, M., Ivanov, L., Ivanova, L., Iversen, C. M., Izquierdo, J., Jackson, R. B., Jackson, B., Jactel, H., Jagodzinski, A. M., Jandt, U., Jansen, S., Jenkins, T., Jentsch, A., Jespersen, J. R. P., Jiang, G. F., Johansen, J. L., Johnson, D., Jokela, E. J., Joly, C. A., Jordan, G. J., Joseph, G. S., Junaedi, D., Junker, R. R., Justes, E., Kabzems, R., Kane, J., Kaplan, Z., Kattenborn, T., Kavelenova, L., Kearsley, E., Kempel, A., Kenzo, T., Kerkhoff, A., Khalil, M. I., Kinlock, N. L., Kissling, W. D., Kitajima, K., Kitzberger, T., Kjøller, R., Klein, T., Kleyer, M., Klimešová, J., Klipel, J., Kloeppel, B., Klotz, S., Knops, J. M., Kohyama, T., Koike, F., Kollmann, J., Komac, B., Komatsu, K., König, C., Kraft, N. J., Kramer, K., Kreft, H., Kühn, I., Kumarathunge, D., Kuppler, J., Kurokawa, H., Kurosawa, Y., Kuyah, S., Laclau, J. P., Lafleur, B., Lallai, E., Lamb, E., Lamprecht, A., Larkin, D. J., Laughlin, D., Le Bagousse-Pinguet, Y., le Maire, G., le Roux, P. C., le Roux, E., Lee, T., Lens, F., Lewis, S. L., Lhotsky, B., Li, Y., Li, X., Lichstein, J. W., Liebergesell, M., Lim, J. Y., Lin, Y. S., Linares, J. C., Liu, C., Liu, D., Liu, U., Livingstone, S., Llusià, J., Lohbeck, M., López-García, Á., Lopez-Gonzalez, G., Lososová, Z., Louault, F., Lukács, B. A., Lukeš, P., Luo, Y., Lussu, M., Ma, S., Maciel Rabelo Pereira, C., Mack, M., Maire, V., Mäkelä, A., Mäkinen, H., Malhado, A. C. M., Mallik, A., Manning, P., Manzoni, S., Marchetti, Z., Marchino, L., Marcilio-Silva, V., Marcon, E., Marignani, M., Markesteijn, L., Martin, A., Martínez-Garza, C., Martínez-Vilalta, J., Mašková, T., Mason, K., Mason, N., Massad, T. J., Masse, J., Mayrose, I., McCarthy, J., McCormack, M. L., McCulloh, K., McFadden, I. R., McGill, B. J., McPartland, M. Y., Medeiros, J. S., Medlyn, B., Meerts, P., Mehrabi, Z., Meir, P., Melo, F. P., Mencuccini, M., Meredieu, C., Messier, J., Mészáros, I., Metsaranta, J., Michaletz, S. T., Michelaki, C., Migalina, S., Milla, R.,

1060   Miller, J. E., Minden, V., Ming, R., Mokany, K., Moles, A. T., Molnár, A., Molofsky, J., Molz, M., Montgomery, R. A., Monty, A., Moravcová, L., Moreno-Martínez, A., Moretti, M., Mori, A. S., Mori, S., Morris, D., Morrison, J., Mucina, L., Mueller, S., Muir, C. D., Müller, S. C., Munoz, F., Myers-Smith, I. H., Myster, R. W., Nagano, M., Naidu, S., Narayanan, A., Natesan, B., Negoita, L., Nelson, A. S., Neuschulz, E. L., Ni, J., Niedrist, G., Nieto, J., Niinemets, Ü., Nolan, R., Nottebrock, H., Nouvellon, Y., Novakovskiy, A., Nystuen, K. O., O'Grady, A., O'Hara, K., O'Reilly-Nugent, A., Oakley, S., Oberhuber, W., Ohtsuka, T., Oliveira, R., Öllerer, K., Olson, M. E.,

1065   Onipchenko, V., Onoda, Y., Onstein, R. E., Ordonez, J. C., Osada, N., Ostonen, I., Ottaviani, G., Otto, S., Overbeck, G. E., Ozinga, W. A., Pahl, A. T., Paine, C. E., Pakeman, R. J., Papageorgiou, A. C., Parfionova, E., Pärtel, M., Patacca, M., Paula, S., Paule, J., Pauli, H., Pausas, J. G., Peco, B., Penuelas, J., Perea, A., Peri, P. L., Petisco-Souza, A. C., Petraglia, A., Petritan, A. M., Phillips, O. L., Pierce, S., Pillar, V. D., Pisek, J., Pomogaybin, A., Poorter, H., Portsmuth, A., Poschlod, P., Potvin, C., Pounds, D., Powell, A. S., Power, S. A., Prinzing, A., Puglielli, G., Pyšek, P., Raevel, V., Rammig, A., Ransijn, J., Ray, C. A., Reich, P. B., Reichstein, M., Reid, D. E., Réjou-Méchain,

1070   M., de Dios, V. R., Ribeiro, S., Richardson, S., Riibak, K., Rillig, M. C., Riviera, F., Robert, E. M., Roberts, S., Robroek, B., Roddy, A., Rodrigues, A. V., Rogers, A., Rollinson, E., Rolo, V., Römermann, C., Ronzhina, D., Roscher, C., Rosell, J. A., Rosenfield, M. F., Rossi, C., Roy, D. B., Royer-Tardif, S., Rüger, N., Ruiz-Peinado, R., Rumpf, S. B., Rusch, G. M., Ryo, M., Sack, L., Saldaña, A., Salgado-Negret, B., Salguero-Gomez, R., Santa-Regina, I., Santacruz-García, A. C., Santos, J., Sardans, J., Schamp, B., Scherer-Lorenzen, M., Schleuning, M., Schmid, B., Schmidt, M., Schmitt, S., Schneider, J. V., Schowanek, S. D., Schrader, J., Schrodt, F., Schuldt, B., Schurr,

1075   F., Selaya Garvizu, G., Semchenko, M., Seymour, C., Sfair, J. C., Sharpe, J. M., Sheppard, C. S., Sheremetiev, S., Shiodera, S., Shipley, B., Shovon, T. A., Siebenkäs, A., Sierra, C., Silva, V., Silva, M., Sitzia, T., Sjöman, H., Slot, M., Smith, N. G., Sodhi, D., Soltis, P., Soltis, D., Somers, B., Sonnier, G., Sørensen, M. V., Sosinski, E. E., Soudzilovskaia, N. A., Souza, A. F., Spasojevic, M., Sperandii, M. G., Stan, A. B., Stegen, J., Steinbauer, K., Stephan, J. G., Sterck, F., Stojanovic, D. B., Strydom, T., Suarez, M. L., Svenning, J. C., Svitková, I., Svitok, M., Svoboda, M., Swaine, E., Swenson, N., Tabarelli, M., Takagi, K., Tappeiner, U., Tarifa, R., Tauugourdeau, S., Tavsanoglu,

1080   C., te Beest, M., Tedersoo, L., Thiffault, N., Thom, D., Thomas, E., Thompson, K., Thornton, P. E., Thuiller, W., Tichý, L., Tissue, D., Tjoelker, M. G., Tng, D. Y. P., Tobias, J., Török, P., Tarin, T., Torres-Ruiz, J. M., Tóthmérész, B., Treurnicht, M., Trivellone, V., Trolliet, F., Trotsiuk, V., Tsakalos, J. L., Tsiripidis, I., Tysklind, N., Umehara, T., Usoltsev, V., Vadeboncoeur, M., Vaezi, J., Valladares, F., Vamosi, J., van Bodegom, P. M., van Breugel, M., Van Cleemput, E., van de Weg, M., van der Merwe, S., van der Plas, F., van der Sande, M. T., van Kleunen, M., Van Meerbeek, K., Vanderwel, M., Vanselow, K. A., Vårhammar, A., Varone, L., Vasquez Valderrama, M. Y., Vassilev, K.,

1085   Vellend, M., Veneklaas, E. J., Verbeeck, H., Verheyen, K., Vibrans, A., Vieira, I., Villacís, J., Violle, C., Vivek, P., Wagner, K., Waldram, M., Waldron, A., Walker, A. P., Waller, M., Walther, G., Wang, H., Wang, F., Wang, W., Watkins, H., Watkins, J., Weber, U., Weedon, J. T., Wei, L., Weigelt, P., Weiher, E., Wells, A. W., Wellstein, C., Wenk, E., Westoby, M., Westwood, A., White, P. J., Whitten, M., Williams, M., Winkler, D. E., Winter, K., Womack, C., Wright, I. J., Wright, S. J., Wright, J., Pinho, B. X., Ximenes, F., Yamada, T., Yamaji, K., Yanai, R., Yankov, N., Yguel, B., Zanini, K. J., Zanne, A. E., Zelený, D., Zhao, Y. P., Zheng, J., Zheng, J., Ziemińska, K., Zirbel, C. R.,

1090   Zizka, G., Zo-Bi, I. C., Zotz, G., and Wirth, C.: TRY plant trait database – enhanced coverage and open access, Global Change Biology, 26, 119–188, https://doi.org/10.1111/gcb.14904, 2020.

Keenan, T., Sabate, S., and Gracia, C.: The importance of mesophyll conductance in regulating forest ecosystem productivity during drought periods, Global Change Biology, 16, 1019–1034, https://doi.org/10.1111/j.1365-2486.2009.02017.x, 2010.

Kling, H., Fuchs, M., and Paulin, M.: Runoff conditions in the upper Danube basin under an ensemble of climate change scenarios, Journal

1095   of Hydrology, 424-425, 264–277, https://doi.org/10.1016/j.jhydrol.2012.01.011, http://dx.doi.org/10.1016/j.jhydrol.2012.01.011, 2012.

Knox, S. H., Sturtevant, C., Matthes, J. H., Koteen, L., Verfaillie, J., and Baldocchi, D.: Agricultural peatland restoration: Effects of land-use change on greenhouse gas (CO_2 and CH_4) fluxes in the Sacramento-San Joaquin Delta, Global Change Biology, 21, 750–765, https://doi.org/10.1111/gcb.12745, 2015.

Koebsch, F., Sonnentag, O., Järveoja, J., Peltoniemi, M., Alekseychik, P., Aurela, M., Arslan, A. N., Dinsmore, K., Gianelle, D., Helfter, C., Jackowicz-Korczynski, M., Korrensalo, A., Leith, F., Linkosalmi, M., Lohila, A., Lund, M., Maddison, M., Mammarella, I., Mander, Ü., Minkkinen, K., Pickard, A., Pullens, J. W., Tuittila, E. S., Nilsson, M. B., and Peichl, M.: Refining the role of phenology in regulating gross ecosystem productivity across European peatlands, Global Change Biology, 26, 876–887, https://doi.org/10.1111/gcb.14905, 2020.

Krinner, G., Viovy, N., de Noblet-Ducoudré, N., Ogée, J., Polcher, J., Friedlingstein, P., Ciais, P., Sitch, S., and Prentice, I. C.: A dynamic global vegetation model for studies of the coupled atmosphere-biosphere system, Global Biogeochemical Cycles, 19, 1–33, https://doi.org/10.1029/2003GB002199, http://doi.wiley.com/10.1029/2003GB002199, 2005.

Lafleur, P. M., Roulet, N. T., Bubier, J. L., Frolking, S., and Moore, T. R.: Interannual variability in the peatland-atmosphere carbon dioxide exchange at an ombrotrophic bog, Global Biogeochemical Cycles, 17, 1–14, https://doi.org/10.1029/2002gb001983, 2003.

Laine, A. M., Korrensalo, A., and Tuittila, E. S.: Plant functional traits play the second fiddle to plant functional types in explaining peatland CO_2 and CH_4 gas exchange, Science of the Total Environment, 834, 155 352, https://doi.org/10.1016/j.scitotenv.2022.155352, https://doi.org/10.1016/j.scitotenv.2022.155352, 2022.

Li, T., Raivonen, M., Alekseychik, P., Aurela, M., Lohila, A., Zheng, X., Zhang, Q., Wang, G., Mammarella, I., Rinne, J., Yu, L., Xie, B., Vesala, T., and Zhang, W.: Importance of vegetation classes in modeling CH_4 emissions from boreal and subarctic wetlands in Finland, Science of the Total Environment, 572, 1111–1122, https://doi.org/10.1016/j.scitotenv.2016.08.020, http://dx.doi.org/10.1016/j.scitotenv.2016.08.020, 2016.

Lippmann, T. J., Zandt, M. H., Van Der Putten, N. N., Busschers, F. S., Hijma, M. P., Van Der Velden, P., De Groot, T., Van Aalderen, Z., Meisel, O. H., Slomp, C. P., Niemann, H., Jetten, M. S., Dolman, H. A., and Welte, C. U.: Microbial activity, methane production, and carbon storage in Early Holocene North Sea peats, Biogeosciences, 18, 5491–5511, https://doi.org/10.5194/bg-18-5491-2021, 2021.

Lippmann, T. J. R. and van Huissteden, J.: Peatland-VU-NUCOM (PVN 1.0): A peatland GHG emissions model using dynamic plant functional types, https://doi.org/https://doi.org/10.5281/zenodo.7701698, https://zenodo.org/record/7701698, 2023.

Littleton, E. W., Harper, A. B., Vaughan, N. E., Oliver, R. J., Duran-Rojas, M. C., and Lenton, T. M.: JULES-BE: Representation of bioenergy crops and harvesting in the Joint UK Land Environment Simulator vn5.1, Geoscientific Model Development, 13, 1123–1136, https://doi.org/10.5194/gmd-13-1123-2020, https://gmd.copernicus.org/articles/13/1123/2020/, 2020.

Loisel, J., Gallego-Sala, A. V., Amesbury, M. J., Magnan, G., Anshari, G., Beilman, D. W., Benavides, J. C., Blewett, J., Camill, P., Charman, D. J., Chawchai, S., Hedgpeth, A., Kleinen, T., Korhola, A., Large, D., Mansilla, C. A., Müller, J., van Bellen, S., West, J. B., Yu, Z., Bubier, J. L., Garneau, M., Moore, T., Sannel, A. B., Page, S., Väliranta, M., Bechtold, M., Brovkin, V., Cole, L. E., Chanton, J. P., Christensen, T. R., Davies, M. A., De Vleeschouwer, F., Finkelstein, S. A., Frolking, S., Gałka, M., Gandois, L., Girkin, N., Harris, L. I., Heinemeyer, A., Hoyt, A. M., Jones, M. C., Joos, F., Juutinen, S., Kaiser, K., Lacourse, T., Lamentowicz, M., Larmola, T., Leifeld, J., Lohila, A., Milner, A. M., Minkkinen, K., Moss, P., Naafs, B. D., Nichols, J., O'Donnell, J., Payne, R., Philben, M., Piilo, S., Quillet, A., Ratnayake, A. S., Roland, T. P., Sjögersten, S., Sonnentag, O., Swindles, G. T., Swinnen, W., Talbot, J., Treat, C., Valach, A. C., and Wu, J.: Expert assessment of future vulnerability of the global peatland carbon sink, Nature Climate Change, 11, 70–77, https://doi.org/10.1038/s41558-020-00944-0, 2021.

Malmer, N., Albinsson, C., Svensson, B. M., and Wallén, B.: Interferences between Sphagnum and vascular plants: Effects on plant community structure and peat formation, Oikos, 100, 469–482, https://doi.org/10.1034/j.1600-0706.2003.12170.x, 2003.

Malmer, N., Johansson, T., Olsrud, M., and Christensen, T. R.: Vegetation, climatic changes and net carbon sequestration in a North-Scandinavian subarctic mire over 30 years, Global Change Biology, 11, 1895–1909, https://doi.org/10.1111/j.1365-2486.2005.01042.x, 2005.

Masson-Delmotte, V., Zhai, P., Pirani, A., Connors, S. L., Péan, C., Berger, S., Caud, N., Chen, Y., Goldfarb, L., Gomis, M. I., Huang, M., Leitzell, K., Lonnoy, E., Matthews, J. B. R., Maycock, T. K., Waterfield, T., Yelekçi, O., Yu, R., and Zhou, B., eds.: Climate Change 2021: The Physical Science Basis. Contribution of Working Group I to the Sixth Assessment Report of the Intergovernmental Panel on Climate Change, vol. In Press, Cambridge University Press, Cambridge, United Kingdom and New York, NY, USA, https://doi.org/10.1017/9781009157896, 2021.

Mazzola, V., Perks, M. P., Smith, J., Yeluripati, J., and Xenakis, G.: Assessing soil carbon dioxide and methane fluxes from a Scots pine raised bog-edge-woodland, Journal of Environmental Management, 302, 114 061, https://doi.org/10.1016/j.jenvman.2021.114061, https://doi.org/10.1016/j.jenvman.2021.114061, 2022.

Melillo, J. M., Steudler, P. A., Aber, J. D., Newkirk, K., Lux, H., Bowles, F. P., Catricala, C., Magill, A., Ahrens, T., and Morrisseau, S.: Soil warming and carbon-cycle feedbacks to the climate system, Science, 298, 2173–2176, https://doi.org/10.1126/science.1074153, 2002.

Melton, J. R., Wania, R., Hodson, E. L., Poulter, B., Ringeval, B., Spahni, R., Bohn, T., Avis, C. A., Beerling, D. J., Chen, G., Eliseev, A. V., Denisov, S. N., Hopcroft, P. O., Lettenmaier, D. P., Riley, W. J., Singarayer, J. S., Subin, Z. M., Tian, H., Zürcher, S., Brovkin, V., van Bodegom, P. M., Kleinen, T., Yu, Z. C., and Kaplan, J. O.: Present state of global wetland extent and wetland methane modelling: conclusions from a model inter-comparison project (WETCHIMP), Biogeosciences, 10, 753–788, https://doi.org/10.5194/bg-10-753-2013, https://bg.copernicus.org/articles/10/753/2013/, 2013.

Metzger, C., Jansson, P. E., Lohila, A., Aurela, M., Eickenscheidt, T., Belelli-Marchesini, L., Dinsmore, K. J., Drewer, J., Van Huissteden, J., and Drösler, M.: CO2 fluxes and ecosystem dynamics at five European treeless peatlands-merging data and process oriented modeling, Biogeosciences, 12, 125–146, https://doi.org/10.5194/bg-12-125-2015, http://www.biogeosciences.net/12/125/2015/https://bg.copernicus.org/articles/12/125/2015/, 2015.

Mi, Y., Van Huissteden, J., Parmentier, F. J. W., Gallagher, A., Budishchev, A., Berridge, C. T., and Dolman, A. J.: Improving a plot-scale methane emission model and its performance at a northeastern Siberian tundra site, Biogeosciences, 11, 3985–3999, https://doi.org/10.5194/bg-11-3985-2014, 2014.

Moore, T. R., Bubier, J. L., and Bledzki, L.: Litter decomposition in temperate peatland ecosystems: The effect of substrate and site, Ecosystems, 10, 949–963, https://doi.org/10.1007/s10021-007-9064-5, http://link.springer.com/10.1007/s10021-007-9064-5, 2007.

Morin, T. H., Bohrer, G., Frasson, R. P., Naor-Azreli, L., Mesi, S., Stefanik, K. C., and Schäfer, K. V.: Environmental drivers of methane fluxes from an urban temperate wetland park, Journal of Geophysical Research: Biogeosciences, 119, 2188–2208, https://doi.org/10.1002/2014JG002750, 2014a.

Morin, T. H., Bohrer, G., Naor-Azrieli, L., Mesi, S., Kenny, W. T., Mitsch, W. J., and Schäfer, K. V. R.: The seasonal and diurnal dynamics of methane flux at a created urban wetland, Ecological Engineering, 72, 74–83, https://doi.org/10.1016/j.ecoleng.2014.02.002, http://dx.doi.org/10.1016/j.ecoleng.2014.02.002, 2014b.

Morin, T. H., Bohrer, G., Stefanik, K. C., Rey-Sanchez, A. C., Matheny, A. M., and Mitsch, W. J.: Combining eddy-covariance and chamber measurements to determine the methane budget from a small, heterogeneous urban floodplain wetland park, Agricultural and Forest Meteorology, 237-238, 160–170, https://doi.org/10.1016/j.agrformet.2017.01.022, http://dx.doi.org/10.1016/j.agrformet.2017.01.022, 2017.

Muñoz-Sabater, J., Dutra, E., Agustí-Panareda, A., Albergel, C., Arduini, G., Balsamo, G., Boussetta, S., Choulga, M., Harrigan, S., Hersbach, H., Martens, B., Miralles, D. G., Piles, M., Rodríguez-Fernández, N. J., Zsoter, E., Buontempo, C., and Thépaut, J. N.: ERA5-Land:

A state-of-the-art global reanalysis dataset for land applications, Earth System Science Data, 13, 4349–4383, https://doi.org/10.5194/essd-13-4349-2021, 2021.

Ostle, N. J., Smith, P., Fisher, R., Ian Woodward, F., Fisher, J. B., Smith, J. U., Galbraith, D., Levy, P., Meir, P., McNamara, N. P., and Bardgett, R. D.: Integrating plant-soil interactions into global carbon cycle models, Journal of Ecology, 97, 851–863, https://doi.org/10.1111/j.1365-2745.2009.01547.x, 2009.

Pangala, S. R., Moore, S., Hornibrook, E. R., and Gauci, V.: Trees are major conduits for methane egress from tropical forested wetlands, New Phytologist, 197, 524–531, https://doi.org/10.1111/nph.12031, 2013.

Peltoniemi, K., Fritze, H., and Laiho, R.: Response of fungal and actinobacterial communities to water-level drawdown in boreal peatland sites, Soil Biology and Biochemistry, 41, 1902–1914, https://doi.org/10.1016/j.soilbio.2009.06.018, http://dx.doi.org/10.1016/j.soilbio.2009.06.018, 2009.

Puma, M. J., Koster, R. D., and Cook, B. I.: Phenological versus meteorological controls on land-atmosphere water and carbon fluxes, Journal of Geophysical Research: Biogeosciences, 118, 14–29, https://doi.org/10.1029/2012JG002088, 2013.

Saarnio, S., Wittenmayer, L., and Merbach, W.: Rhizospheric exudation of Eriophorum vaginatum L. — Potential link to methanogenesis, Plant and Soil, 267, 343–355, https://doi.org/10.1007/s11104-005-0140-3, 2004.

Saleska, S. R., Shaw, M. R., Fischer, M. L., Dunne, J. A., Still, C. J., Holman, M. L., and Harte, J.: Plant community composition mediates both large transient decline and predicted long-term recovery of soil carbon under climate warming, Global Biogeochemical Cycles, 16, 3–1–3–18, https://doi.org/10.1029/2001gb001573, 2002.

Schipper, L. A. and Reddy, K. R.: Determination of Methane Oxidation in the Rhizosphere of Sagittaria lancifolia Using Methyl Fluoride, Soil Science Society of America Journal, 60, 611–616, https://doi.org/10.2136/sssaj1996.03615995006000020039x, 1996.

Schrier-Uijl, A. P., Kroon, P. S., Hendriks, D. M. D., Hensen, A., Van Huissteden, J., Berendse, F., and Veenendaal, E. M.: Agricultural peatlands: Towards a greenhouse gas sink - A synthesis of a Dutch landscape study, Biogeosciences, 11, 4559–4576, https://doi.org/10.5194/bg-11-4559-2014, 2014.

Sitch, S., Smith, B., Prentice, I. C., Arneth, A., Bondeau, A., Cramer, W., Kaplan, J. O., Levis, S., Lucht, W., Sykes, M. T., Thonicke, K., and Venevsky, S.: Evaluation of ecosystem dynamics, plant geography and terrestrial carbon cycling in the LPJ dynamic global vegetation model, Global Change Biology, 9, 161–185, https://doi.org/10.1046/j.1365-2486.2003.00569.x, 2003.

Smith, B., Prentice, I. C., and Sykes, M. T.: Representation of vegetation dynamics in the modelling of terrestrial ecosystems: comparing two contrasting approaches within European climate space, Global Ecology and Biogeography, 10, 621–637, https://doi.org/10.1046/j.1466-822x.2001.t01-1-00256.x, 2001.

Smithwick, E. A., Lucash, M. S., McCormack, M. L., and Sivandran, G.: Improving the representation of roots in terrestrial models, Ecological Modelling, 291, 193–204, https://doi.org/10.1016/j.ecolmodel.2014.07.023, http://dx.doi.org/10.1016/j.ecolmodel.2014.07.023, 2014.

Speckman, H. N., Frank, J. M., Bradford, J. B., Miles, B. L., Massman, W. J., Parton, W. J., and Ryan, M. G.: Forest ecosystem respiration estimated from eddy covariance and chamber measurements under high turbulence and substantial tree mortality from bark beetles, Global Change Biology, 21, 708–721, https://doi.org/10.1111/gcb.12731, 2015.

Strack, M., Waller, M. F., and Waddington, J. M.: Sedge succession and peatland methane dynamics: A potential feedback to climate change, Ecosystems, 9, 278–287, https://doi.org/10.1007/s10021-005-0070-1, 2006.

Ström, L., Mastepanov, M., and Christensen, T. R.: Species-specific Effects of Vascular Plants on Carbon Turnover and Methane Emissions from Wetlands, Biogeochemistry, 75, 65–82, https://doi.org/10.1007/s10533-004-6124-1, https://doi.org/10.1007/s10533-004-6124-1http://link.springer.com/10.1007/s10533-004-6124-1, 2005.

1210   Ström, L., Falk, J. M., Skov, K., Jackowicz-Korczynski, M., Mastepanov, M., Christensen, T. R., Lund, M., and Schmidt, N. M.: Controls of spatial and temporal variability in CH4 flux in a high arctic fen over three years, Biogeochemistry, 125, 21–35, https://doi.org/10.1007/s10533-015-0109-0, 2015.

Tiemeyer, B., Albiac Borraz, E., Augustin, J., Bechtold, M., Beetz, S., Beyer, C., Drosler, M., Ebli, M., Eickenscheidt, T., Fiedler, S., Forster, C., Freibauer, A., Giebels, M., Glatzel, S., Heinichen, J., Hoffmann, M., Hoper, H., Jurasinski, G., Leiber-Sauheitl, K., Peichl-Brak, M.,
1215   Rosskopf, N., Sommer, M., and Zeitz, J.: High emissions of greenhouse gases from grasslands on peat and other organic soils, Global Change Biology, 22, 4134–4149, https://doi.org/10.1111/gcb.13303, 2016.

Toet, S., Cornelissen, J. H., Aerts, R., Van Logtestijn, R. S., De Beus, M., and Stoevelaar, R.: Moss responses to elevated CO2 and variation in hydrology in a temperate lowland peatland, Plant Ecology, 182, 27–40, https://doi.org/10.1007/s11258-005-9029-8, 2006.

Tramontana, G., Jung, M., Schwalm, C. R., Ichii, K., Camps-Valls, G., Ráduly, B., Reichstein, M., Arain, M. A., Cescatti, A., Kiely, G.,
1220   Merbold, L., Serrano-Ortiz, P., Sickert, S., Wolf, S., and Papale, D.: Predicting carbon dioxide and energy fluxes across global FLUXNET sites with regression algorithms, Biogeosciences, 13, 4291–4313, https://doi.org/10.5194/bg-13-4291-2016, 2016.

Van den Hoof, C., Hanert, E., and Vidale, P. L.: Simulating dynamic crop growth with an adapted land surface model - JULES-SUCROS: Model development and validation, Agricultural and Forest Meteorology, 151, 137–153, https://doi.org/10.1016/j.agrformet.2010.09.011, https://linkinghub.elsevier.com/retrieve/pii/S0168192310002571, 2011.

1225   van Geel, B., Bos, J. M., and Pals, J. P.: Archaeological and palaeoecological aspects of a medieval house terp in a reclaimed raiseg bog area in North Holland, Ber. Rijksd. Oudheidkd. Bodemonderz, 33, 419–444, 1983.

van Huissteden, J., van den Bos, R., and Marticorena Alvarez, I.: Modelling the effect of water-table management on CO2 and CH4 fluxes from peat soils, Geologie en Mijnbouw/Netherlands Journal of Geosciences, 85, 3–18, https://doi.org/10.1017/S0016774600021399, 2006.

1230   van Huissteden, J., Petrescu, a. M. R., Hendriks, D. M. D., and Rebel, K. T.: Sensitivity analysis of a wetland methane emission model based on temperate and Arctic wetland sites, Biogeosciences, 6, 9083–9126, https://doi.org/10.5194/bgd-6-9083-2009, 2009.

Waddington, J. M. and Roulet, N. T.: Carbon balance of a Boreal patterned peatland, Global Change Biology, 6, 87–97, https://doi.org/10.1046/j.1365-2486.2000.00283.x, 2000.

Waldo, N. B., Hunt, B. K., Fadely, E. C., Moran, J. J., and Neumann, R. B.: Plant root exudates increase methane emissions through
1235   direct and indirect pathways, Biogeochemistry, 145, 213–234, https://doi.org/10.1007/s10533-019-00600-6, https://doi.org/10.1007/s10533-019-00600-6, 2019.

Walter, B. P. and Heimann, M.: A process-based, climate-sensitive model to derive methane emissions from natural wetlands: Application to five wetland sites, sensitivity to model parameters, and climate, Global Biogeochemical Cycles, 14, 745–765, https://doi.org/10.1029/1999GB001204, 2000.

1240   Wania, R., Ross, I., and Prentice, I. C.: Implementation and evaluation of a new methane model within a dynamic global vegetation model: LPJ-WHyMe v1.3.1, Geoscientific Model Development, 3, 565–584, https://doi.org/10.5194/gmd-3-565-2010, 2010.

Wania, R., Melton, J. R., Hodson, E. L., Poulter, B., Ringeval, B., Spahni, R., Bohn, T., Avis, C. A., Chen, G., Eliseev, A. V., Hopcroft, P. O., Riley, W. J., Subin, Z. M., Tian, H., Van Bodegom, P. M., Kleinen, T., Yu, Z. C., Singarayer, J. S., Zürcher, S., Lettenmaier, D. P., Beerling, D. J., Denisov, S. N., Prigent, C., Papa, F., and Kaplan, J. O.: Present state of global wetland extent and wetland
1245   methane modelling: Methodology of a model inter-comparison project (WETCHIMP), Geoscientific Model Development, 6, 617–641, https://doi.org/10.5194/gmd-6-617-2013, 2013.

WGI, I. A.: Climate Change 2021 The Physical Science Basis WGI, vol. 34, 2021.

Whipps, J. M.: Carbon economy., The rhizosphere., pp. 59–97, 1990.

Wu, Y. and Blodau, C.: PEATBOG: a biogeochemical model for analyzing coupled carbon and nitrogen dynamics in northern peatlands, Geoscientific Model Development, 6, 1173–1207, https://doi.org/10.5194/gmd-6-1173-2013, https://gmd.copernicus.org/articles/6/1173/2013/, 2013.

Wu, Y., Verseghy, D. L., and Melton, J. R.: Integrating peatlands into the coupled Canadian Land Surface Scheme (CLASS) v3.6 and the Canadian Terrestrial Ecosystem Model (CTEM) v2.0, Geoscientific Model Development, 9, 2639–2663, https://doi.org/10.5194/gmd-9-2639-2016, https://gmd.copernicus.org/articles/9/2639/2016/, 2016.

Wullschleger, S. D., Epstein, H. E., Box, E. O., Euskirchen, E. S., Goswami, S., Iversen, C. M., Kattge, J., Norby, R. J., Van Bodegom, P. M., and Xu, X.: Plant functional types in Earth system models: Past experiences and future directions for application of dynamic vegetation models in high-latitude ecosystems, Annals of Botany, 114, 1–16, https://doi.org/10.1093/aob/mcu077, https://academic.oup.com/aob/article-lookup/doi/10.1093/aob/mcu077, 2014.

Yrjälä, K., Tuomivirta, T., Juottonen, H., Putkinen, A., Lappi, K., Tuittila, E. S., Penttilä, T., Minkkinen, K., Laine, J., Peltoniemi, K., and Fritze, H.: CH4 production and oxidation processes in a boreal fen ecosystem after long-term water table drawdown, Global Change Biology, 17, 1311–1320, https://doi.org/10.1111/j.1365-2486.2010.02290.x, 2011.

Yu, Z., Loisel, J., Brosseau, D. P., Beilman, D. W., and Hunt, S. J.: Global peatland dynamics since the Last Glacial Maximum, Geophysical Research Letters, 37, 1–5, https://doi.org/10.1029/2010GL043584, 2010.

Zeng, X.: Global Vegetation Root Distribution for Land Modeling, Journal of Hydrometeorology, 2, 525–530, https://doi.org/10.1175/1525-7541(2001)002<0525:gvrdfl>2.0.co;2, 2001.

Zhao, J., Lange, H., and Meissner, H.: Gap-filling continuously-measured soil respiration data: A highlight of time-series-based methods, Agricultural and Forest Meteorology, 285-286, 107 912, https://doi.org/10.1016/j.agrformet.2020.107912, https://doi.org/10.1016/j.agrformet.2020.107912, 2020.